Targeting human Mas-related G protein-coupled receptor X1 to inhibit persistent pain

Zhe Li[a,1], Pang-Yen Tseng[a,1], Vinod Tiwari[b,1], Qian Xu[a], Shao-Qiu He[b], Yan Wang[a], Qin Zheng[a], Liang Han[a], Zhiping Wu[c,d], Anna L. Blobaum[e], Yiyuan Cui[f], Vineeta Tiwari[b], Shuohao Sun[a], Yingying Cheng[a], Julie H. Y. Huang-Lionnet[b], Yixun Geng[a], Bo Xiao[f], Junmin Peng[c,d,g], Corey Hopkins[e], Srinivasa N. Raja[b], Yun Guan[b,2], and Xinzhong Dong[a,h,2]

[a]The Solomon H. Snyder Department of Neuroscience, Center for Sensory Biology, Johns Hopkins University School of Medicine, Baltimore, MD 21205; [b]Department of Anesthesiology and Critical Care Medicine, Johns Hopkins University School of Medicine, Baltimore, MD 21205; [c]Department of Structural Biology, St. Jude Children's Research Hospital, Memphis, TN 38105; [d]Department of Developmental Neurobiology, St. Jude Children's Research Hospital, Memphis, TN 38105; [e]Department of Pharmacology, Vanderbilt Center for Neuroscience Drug Discovery, Vanderbilt Specialized Chemistry Center, Vanderbilt University Medical Center, Nashville, TN 37232; [f]The State Key Laboratory of Biotherapy, West China Hospital, Sichuan University, Chengdu, People's Republic of China; [g]St. Jude Proteomics Facility, St. Jude Children's Research Hospital, Memphis, TN 38105; and [h]Howard Hughes Medical Institute, Johns Hopkins University School of Medicine, Baltimore, MD 21205

Human Mas-related G protein-coupled receptor X1 (MRGPRX1) is a promising target for pain inhibition, mainly because of its restricted expression in nociceptors within the peripheral nervous system. However, constrained by species differences across Mrgprs, drug candidates that activate MRGPRX1 do not activate rodent receptors, leaving no responsive animal model to test the effect on pain in vivo. Here, we generated a transgenic mouse line in which we replaced mouse Mrgprs with human MrgprX1. This humanized mouse allowed us to characterize an agonist [bovine adrenal medulla 8–22 (BAM8–22)] and a positive allosteric modulator (PAM), ML382, of MRGPRX1. Cellular studies suggested that ML382 enhances the ability of BAM8–22 to inhibit high-voltage-activated Ca^{2+} channels and attenuate spinal nociceptive transmission. Importantly, both BAM8–22 and ML382 effectively attenuated evoked, persistent, and spontaneous pain without causing obvious side effects. Notably, ML382 by itself attenuated both evoked pain hypersensitivity and spontaneous pain in MrgprX1 mice after nerve injury without acquiring coadministration of an exogenous agonist. Our findings suggest that humanized MrgprX1 mice provide a promising preclinical model and that activating MRGPRX1 is an effective way to treat persistent pain.

pain | DRG neurons | MrgprX1 | GPCR | positive allosteric modulator

Persistent pain is a major healthcare problem that remains difficult to manage. Commonly used analgesics (e.g., opioids) often lead to an array of adverse side effects (e.g., sedation, addiction, toxicity) that further deteriorate life quality (1, 2). An important reason why most pain medicines produce dose-limiting side effects is the broad expression of drug targets (e.g., opioid receptors, cyclooxygenase-2) in the central nervous system (CNS) and outside of pain pathways (e.g., cardiovascular system) (3). Because persistent pain is often primed with peripheral pathological conditions, such as tissue inflammation and nerve injury, and its maintenance is also attributable to peripheral neuronal sensitization (4, 5), development of pain-specific treatments would greatly benefit from the identification of novel targets specifically expressed in pain pathways, especially those targets on nociceptive primary sensory neurons (6).

One potential target is the Mas-related G protein-coupled receptor (MRGPR). MRGPRs comprise a family of orphan G protein-coupled receptors (GPCRs) and include many genes in humans and rodents (7–11), but their physiological functions are only partially known. Many Mrgpr genes (mouse MrgprA3, MrgprC11, and MrgprD; rat MrgprC; and human MrgprX1) are expressed specifically in small-diameter primary sensory dorsal root ganglia (DRG) neurons (presumably nociceptive) in rodents, monkeys, and humans discovered using various approaches, and have been reported to play important roles in pain and itch (6, 10, 12–19).

Animal studies suggest that a potential drug target is the MRGPRC in trigeminal ganglia and DRG (6, 20, 21). Activation of MRGPRC with agonists by intrathecal (i.th.) application attenuates inflammatory and neuropathic pain-related behavior in rodent models (6, 21). In contrast, Mrgpr-clusterΔ[−/−] (Mrgpr^{−/−}) mice, which have a deletion of 12 Mrgprs, including MrgprA3 and MrgprC11, display enhanced inflammatory (21) and prolonged neuropathic pain (14). These data suggest that MRGPRC at central terminals of primary sensory neurons may function as an endogenous pain inhibitor mechanism in rodents. To facilitate future translational studies, it is imperative to examine how data obtained from rodent MRGPRC studies can be extended to human MRGPRX1. However, the functional properties of MRGPRX1 cannot be fully inferred from MRGPRC owing to cross-species variation in MRGPR agonist activity and receptor function. Although MrgprC is also annotated by the National Center for Biotechnology Information database as mouse MrgprX1 based on the human and mouse sequence

Significance

Chronic pain is a major health and economic problem worldwide with an estimated prevalence reaching epidemic levels of >25% of the population. Most drugs on the market for chronic pain have undesired side effects because their targets exist both inside and outside the pain pathways. Human Mas-related G protein-coupled receptor X1 (MRGPRX1) is a promising target of novel pain inhibitors, mainly because of its restricted expression in primary nociceptive neurons. Our humanized mouse model expressing MRGPRX1 in native nociceptive neurons allowed us to examine physiological roles of MRGPRX1 and to develop therapeutic agents for pain treatment in patients. Our studies suggest that both agonists and positive allosteric modulators of MRGPRX1 may be promising novel drug candidates for managing persistent pain conditions.

homology, it is becoming clear that human MRGPRX1 has binding and pharmacological profiles distinct from the binding and pharmacological profiles of rodent MRGPRC (22). For example, although the sequence of bovine adrenal medulla (BAM) peptide is conserved from rodents to humans (23) (e.g., BAM8–22 activates both MRGPRX1 and MRGPRC) (10, 24), most MRGPRX1-selective agonists have weak or no agonist activity at MRGPRC and do not affect rodent pain behavior (25). Thus, it is not feasible to use conventional animal models to examine the effects of human MRGPRX1 ligands on pain behavior.

Because of the limitations described above, MRGPRX1 functions had only been inferred in previous studies by heterologous overexpression of MRGPRX1 in vitro. However, this approach may alter the binding properties and intracellular signaling (e.g., G protein coupling) of MRGPRX1 (26, 27). Therefore, it remains unclear how MRGPRX1 regulates activities in native primary sensory neurons, and thus pain behavior, in vivo. Here, we report the generation of a transgenic mouse line in which the *MrgprX1* gene is selectively expressed in *MrgprC11*-expressing DRG neurons. This "humanized" mouse line allowed us to examine the effects of an MRGPRX1 full agonist (BAM8–22) and positive allosteric modulator (PAM; ML382) on calcium channel activity in native DRG neurons and on pain behavior (28). In *MrgprX1* mice, BAM8–22 inhibited N-type high-voltage-activated (HVA) calcium current (I_{ca}) in DRG neurons mostly through $G_{\alpha i}$-dependent mechanisms, and attenuated synaptic transmission to high-threshold afferent inputs in lamina II dorsal horn neurons. Importantly, i.th. infusion of BAM8–22 alleviated both evoked pain hypersensitivity and spontaneous pain in these mice after injury. Furthermore, these actions of BAM8–22 were significantly potentiated by cotreatment with ML382 in an MRGPRX1-dependent manner. Allosteric modulators are promising drug candidates for GPCRs. They bind to the allosteric site and modulate the responsiveness of the receptor to the orthosteric ligand (29, 30). Intriguingly, BAM22, an endogenous peptide that can activate MRGPRX1, is significantly increased in the spinal cord after tissue inflammation and nerve injury. Strikingly, i.th. ML382 alone could effectively attenuate both evoked pain and spontaneous pain in *MrgprX1* mice after injury, without causing notable side effects, such as itch. Collectively, our studies suggest that both agonists (e.g., BAM peptides) and PAMs (e.g., ML382) of human MRGPRX1 may be novel drug candidates for managing persistent pain conditions.

Results

Generation of Humanized *MrgprX1* Mice. Human *MrgprX1* is expressed only in subsets of small-diameter sensory neurons in DRG and trigeminal ganglia (7). To establish a mouse model that resembles human MRGPRX1 signaling, we generated a bacterial artificial chromosome (BAC) transgenic *MrgprX1* mouse line. To restrict the expression of *MrgprX1* to the rodent homolog *MrgprC*-expressing neuronal subset, we designed the construct so that *MrgprX1* expression would be driven by the mouse *MrgprC11* promoter (7, 10, 24) (Fig. 1A). The *MrgprC11*[MrgprX1] transgenic line was then mated to the *MrgprA3*[GFP-Cre] transgenic line in which the green fluorescent protein (GFP)-Cre fusion protein is driven by *MrgprA3* promoter (13). Because *MrgprA3* and *MrgprC11* are coexpressed in largely overlapping subsets of DRG neurons (13), we were able to identify the neurons expressing *MrgprX1* transgene for cellular recording by intrinsic GFP fluorescence. Finally, we mated these lines with *Mrgpr*^{−/−} mice, which have an 845-kb deletion that removes 12 endogenous *Mrgpr* genes, including both *MrgprC11* and *MrgprA3* (15). Thus, only *MrgprX1* is expressed in the resulting *Mrgpr*^{−/−}; *MrgprC11*[MrgprX1]; *MrgprA3*[GFP-Cre] mouse line, or *MrgprX1* mice for short. *MrgprX1* mice are viable, fertile, and generally indistinguishable from wild-type littermates. Immunostaining with an anti-MRGPRX1 antibody that we recently generated showed robust expression of MRGPRX1 in a subset of DRG neurons from *MrgprX1* mice but not in *Mrgpr*^{−/−} mice (Fig. 1A). Using RT-PCR,
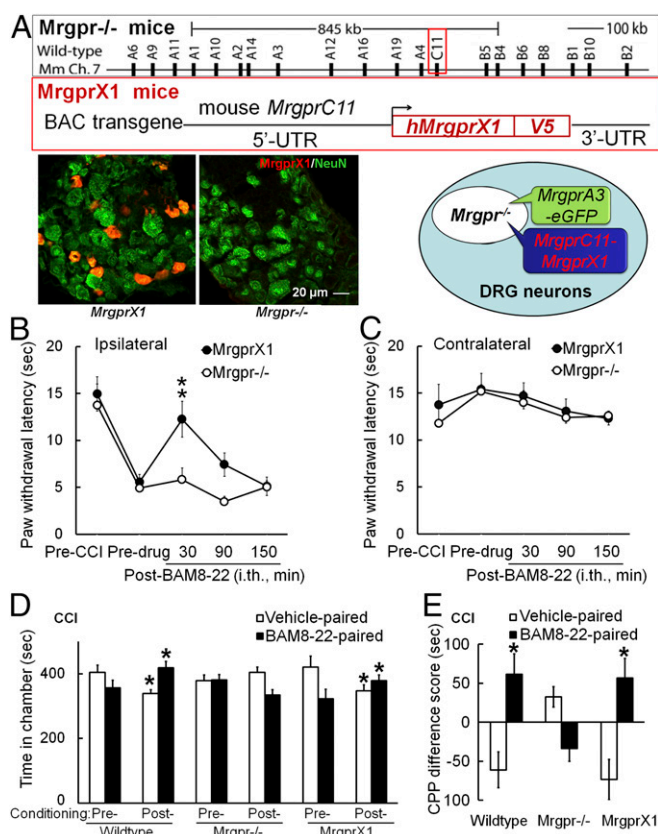

Fig. 1. I.th. administration of BAM8–22 inhibits neuropathic pain-related behavior in *MrgprX1*, but not *Mrgpr*^{−/−} mice. (A, *Upper*) Generation of humanized *MrgprX1* mouse line. The BAC DNA construct for *Mrgpr*^{−/−} mice to express human *MrgprX1* driven by mouse *MrgprC11* promoter is shown. (A, *Lower*) DRG neurons from *Mrgpr*^{−/−} mice with and without *MrgprX1* transgene were stained with anti-MRGPRX1 (red) and anti-NeuN (neuronal marker, green) antibodies. *Mrgprc11*[MrgprX1] transgenic mice were mated with *MrgprA3*[GFP-Cre] transgenic mice and then crossed into the *Mrgpr*^{−/−} background. Therefore, the *MrgprA3*-GFP+ neurons, which are a small subset of all of the DRG neurons, express human MRGPRX1, but not mouse endogenous MRGPRs. (B) At 2–3 wk after CCI of the sciatic nerve, the PWL to radiant heat stimulation was decreased from the preinjury baseline in the ipsilateral hind paw. The heat hypersensitivity in the ipsilateral hind paw was attenuated at 30 min after i.th. administration of BAM8–22 (0.5 mM, 5 μL, i.th.) in *MrgprX1* mice, but not in *Mrgpr*^{−/−} mice. **$P < 0.01$ vs. predrug ($n = 8$ per group), two-way mixed-model ANOVA with a Bonferroni post hoc test. (C) Contralateral PWL was not altered by BAM8–22 treatment in either group. (D) On days 7–13 post-CCI, after conditioning drug treatment, wild-type ($n = 12$) and *MrgprX1* mice ($n = 12$) spent more time in the chamber paired with BAM8–22 (0.5 mM, 5 μL, i.th.) and less time in the vehicle-paired chamber, compared with time spent during the preconditioning test period. BAM8–22 did not induce CPP in *Mrgpr*^{−/−} mice after CCI ($n = 11$). *$P < 0.05$ vs. preconditioning, two-way repeated-measures ANOVA in each genotype with a Bonferroni post hoc test. (E) Difference scores [(Postconditioning time) − (Preconditioning time)] in the BAM8–22-paired chamber were significantly greater than difference scores in vehicle-paired chambers for wild-type and *MrgprX1* mice. *$P < 0.05$ vs. vehicle, paired *t* test.

we detected the *MrgprX1* gene only in DRG, but not in the spinal cord or brain, of *MrgprX1* mice or in DRG of wild-type mice (*SI Appendix*, Fig. S1). Thus, human MRGPRX1 is selectively expressed in DRG neurons of *MrgprX1* mice.

BAM8–22 Inhibited Heat Hypersensitivity and Spontaneous Pain in *MrgprX1* Mice After Peripheral Nerve Injury. We first examined whether MRGPRX1 is systemically functional by testing whether the agonist BAM8–22 attenuates neuropathic pain-related behaviors. In

MrgprX1 mice that had undergone chronic constriction injury (CCI) of the sciatic nerve, i.th. injection of BAM8–22 (0.5 mM, 5 μL; $n = 8$ per group) normalized the decreased ipsilateral paw withdrawal latency (PWL) to noxious heat stimuli at 30 min after injection (Fig. 1*B*), suggesting that BAM8–22 inhibits neuropathic heat hypersensitivity in *MrgprX1* mice. However, this drug effect was absent in *Mrgpr*$^{-/-}$ mice after CCI (Fig. 1*B*). BAM8–22 treatment did not affect the contralateral PWL in either group (Fig. 1*C*).

Clinically, spontaneous or ongoing pain is a debilitating aspect of neuropathic pain caused by spontaneous discharge in somatosensory neurons after nerve injury (31). It can be studied in rodents with a conditioned place preference (CPP) paradigm, which unveils the rewarding effect of relief from ongoing pain (32). At day 7–13 post-CCI, both wild-type and *MrgprX1* mice that received an i.th. injection of BAM8–22 (0.5 mM, 5 μL) during conditioning treatment spent significantly more time in the BAM8–22-paired chamber during the postconditioning phase than they had during the preconditioning phase (Fig. 1*D*). Simultaneously, the mice decreased time spent in the vehicle (saline)-paired chamber. However, *Mrgpr*$^{-/-}$ mice showed no significant change in postconditioning time spent in the BAM8–22- or vehicle-paired chamber, compared with preconditioning (Fig. 1*D*). The difference score also suggested that both wild-type and *MrgprX1* mice showed a preference for the BAM8–22-paired chamber (Fig. 1*E*), whereas *Mrgpr*$^{-/-}$ mice showed neither preference nor aversion to BAM8–22 treatment. These results suggest that BAM8–22 may alleviate ongoing pain in *MrgprX1* mice after nerve injury.

CCI mice dosed with i.th. clonidine (1 μg, 5 μL) were used as positive controls for CPP, and clonidine-treated, sham-operated mice acted as negative controls. Clonidine successfully induced CPP in nerve-injured mice, but not in sham-operated mice, regardless of *Mrgpr* genotype (*SI Appendix*, Fig. S2).

BAM8–22 Inhibited N-Type and P/Q-Type HVA Calcium Channels in Native DRG Neurons Expressing MRGPRX1 Through a Pertussis Toxin-Sensitive Mechanism. We then examined if MRGPRX1 is functional at the cellular level. Activation of $Ca_V2.2$ N-type HVA calcium channels at central terminals of primary sensory neurons is critical to excitatory neurotransmitter release into the spinal cord, which transduces sensory information toward the CNS (33, 34). DRG neurons express at least three types of HVA Ca^{2+} channels, namely, $Ca_V2.2$ N-type, $Ca_V2.1$ P/Q-type, and $Ca_V 1.1/Ca_V 1.4$ L-type (35, 36). Each can be isolated by a specific blocker (33, 37). Inhibiting N-type channels has been well acknowledged to relieve pain (38). Many GPCRs, including mu-opioid receptors; adenosine A1 receptors; and, recently, MRGPRCs, are known to couple to N-type channels and mediate a reduction in Ca^{2+}-dependent presynaptic neurotransmitter release to attenuate spinal nociceptive transmission (39–42). However, how activation of MRGPRX1 affects different subtypes of calcium channels in native DRG neurons has not been directly tested.

In acutely dissociated DRG neurons from *MrgprX1* mice, we recorded I_{Ca} in neurons that coexpress *MrgprA3*-driven GFP and MRGPRX1. All GFP-expressing neurons that we recorded responded to BAM8–22, which is highly potent and specific to MRGPRX1 and rodent MRGPRC (10). We used a protocol to record both low-voltage-activated (LVA) and HVA calcium channels, as shown in Fig. 2*A* (26). All of the *MrgprA3*-GFP$^+$ neurons dominantly expressed HVA I_{ca}, but very few expressed LVA I_{ca} (LVA $I_{Ca} = -20.17 \pm 2.57$ pA; $n = 35$). We found that all three types of HVA calcium channels were present in *MrgprA3*-GFP–labeled neurons (Fig. 2 *A* and *B*). BAM8–22 inhibited HVA I_{Ca}, rapidly and reversibly. To identify which calcium channel is the downstream target of MRGPRX1, we used ω-conotoxin GVIA, ω-agatoxin, and nimodipine to block N-type, P/Q-type, and L-type HVA Ca^{2+} channels, respectively. We applied each blocker individually and tested whether subsequent BAM8–22-induced HVA I_{Ca} inhibition was precluded by the

blocker. Application of 1 μM ω-conotoxin GVIA significantly decreased BAM8–22-induced inhibition from 52.2 to 10.0%, suggesting that the N-type calcium channel is an important target of MRGPRX1 (Fig. 2*C* and *SI Appendix*, Fig. S3*A*). In addition, 0.5 μM ω-agatoxin reduced the effect of BAM8–22 by 43.5%, whereas 10 μM nimodipine did not (Fig. 2*C* and *SI Appendix*, Fig. S3 *B* and *C*), suggesting that P/Q-type calcium channels may also play a partial role but that L-type calcium channels are unlikely to be affected by MRGPRX1.

G protein-mediated inhibition of HVA calcium channels is often coupled to the pertussis toxin (PTX)-sensitive $G_{i/o}$ pathway (26, 43) and involves $G\beta\gamma$ binding to the intracellular loop in a voltage-dependent manner (44–46). To identify downstream G protein pathways further, we used PTX, cholera toxin (CTX), and U73122 to differentiate three types of G protein signaling, namely, $G_{i/o}$, G_s, and phospholipase C. Pretreatment with 2 μg/mL PTX completely abolished BAM8–22-induced inhibition of HVA I_{Ca} (from 50.2 to 1.5%; Fig. 3 *A* and *D*). In contrast, pretreatment with 2 μg/mL CTX or 5 μg/mL U73122 did not significantly reduce BAM8–22-induced inhibition (Fig. 3 *B–D*). To investigate the role of $G\beta\gamma$ binding, we examined the effect of BAM8–22 with a sandwich stimulation protocol, a pair of activation pulses with a strong depolarizing intermediate pulse (43, 44) (*SI Appendix*, Fig. S4*A*). If the effect of BAM8–22 is mediated by $G\beta\gamma$ binding, the strong depolarizing prepulse will relieve $G\beta\gamma$ binding and reverse the inhibition. Indeed, the strong depolarizing prepulse reversed 50% of BAM–22-induced inhibition (*SI Appendix*, Fig. S4*B*). The voltage-dependent activation curve (P-V curve) showed that this voltage protocol fully reversed the voltage dependence of the channel (*SI Appendix*, Fig. S4*C*); therefore, the remaining inhibition was voltage-independent. These results suggest that the inhibition of HVA I_{Ca} by BAM8–22 is partially mediated by $G_{i/o}$-sensitive $G\beta\gamma$ binding of HVA calcium channels and may also involve a $G\beta\gamma$-independent pathway.

ML382 Is a PAM of MRGPRX1 That Enhances the Inhibition of HVA I_{ca} by BAM8–22 in Native DRG Neurons. ML382 was recently suggested to be a PAM of MRGPRX1 in a HEK 293 cell system (28). Its action and specificity to MRGPRX1 remain to be validated in native DRG neurons that endogenously express MRGPRX1. ML382 (5 μM) significantly increased inhibition of I_{Ca} by a low concentration of BAM8–22 (0.5 μM; Fig. 4 *A–C*). However, if BAM8–22 was at a saturating concentration (5 μM), ML382 did not further enhance its inhibition of I_{Ca} (Fig. 4*C*; $n = 6$–8 per group). The I_{Ca} inhibition by BAM8–22 was voltage-dependent, and the voltage dependency of the activation curve shifted to a more positive membrane potential, which reduces the channel open probability after BAM8–22. ML382 positively shifted the activation curve even more in the presence of subsaturating, but not saturating, concentrations of BAM8–22 (Fig. 4*D*). Importantly, ML382 did not inhibit I_{Ca} or shift the voltage dependency in the absence of BAM8–22 (Fig. 4 *E–G*). We tested a higher dose (100 μM) of ML382 in the absence of BAM8–22 to ensure the allosteric modulator itself has no direct effect. In fact, it slightly increased HVA I_{Ca} by $1.4 \pm 2.8\%$ ($n = 7$, evoked by depolarization to -10 mV). Our control, vehicle (extracellular solution), inhibited HVA I_{Ca} by $0.3 \pm 2.8\%$ ($n = 7$), which is not significantly different from 100 μM ML382's effect ($P = 0.59$, paired *t* test). Together, these data suggest that ML382 is a PAM and not an agonist of MRGPRX1.

To confirm further that ML382 allosterically modulates MRGPRX1, we established dose–response curves of BAM8–22 in the presence of different concentrations of ML382, again using GFP-labeled DRG neurons from *MrgprX1* mice (*SI Appendix*, Fig. S5*A*). The dose–response curves were then fitted with the Hill equation. In the absence of ML382, the IC_{50} for BAM8–22 inhibition of I_{Ca} was 0.66 ± 0.05 μM. In the presence of 0.1 μM, 1 μM, 10 μM, and 30 μM ML382, BAM8–22 IC_{50} was reduced to 0.43 ± 0.02 μM, 0.25 ± 0.02 μM, 0.06 ± 0.01 μM, and 0.08 ± 0.01 μM,
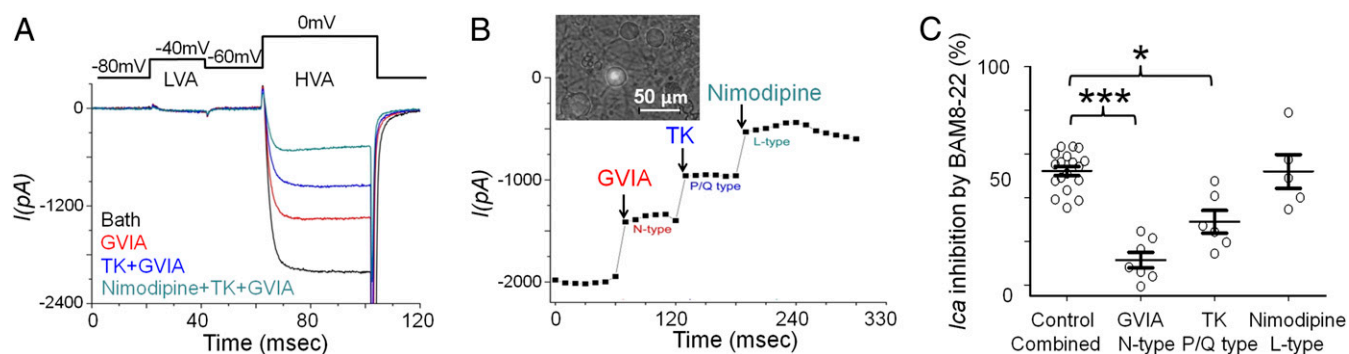
Fig. 2. *MrgprX1* activation inhibits N-type and P/Q-type HVA I_{Ca} in native DRG neurons. (*A, Upper*) Diagram shows that LVA I_{Ca} was evoked at −40 mV (20 ms) from a holding potential of −80 mV and that HVA I_{Ca} was evoked at 10 mV (20 ms) from a holding potential of −60 mV or −80 mV. (*A, Lower*) Representative trace shows the different components of HVA I_{Ca} (*I*) separated by the respective HVA calcium blockers (GVIA, 1 µM; ω-agatoxin TK, 0.5 µM; nimodipine, 10 µM). (*B*) Representative time course of the effects of different HVA calcium channel blockers on HVA I_{Ca} shows that the inhibition is rapid and steady. (*Inset*) Bright-field image shows GFP⁺ neurons, which were used for electrophysiology experiments. (*C*) Amplitude of BAM8–22–induced HVA I_{Ca} inhibition in the presence of different HVA calcium channel blockers (GVIA, 1 µM; TK, 0.5 µM; nimodipine, 10 µM) and vehicle control, normalized by baseline amplitude of HVA I_{Ca} in the same neuron without blockers or BAM8–22 (10 µM). Controls are presented as a combined group. ***$P < 0.001$, *$P < 0.05$ vs. the respective vehicle control, paired *t* test (*n* = 5–7 neurons per group).

respectively (*SI Appendix*, Fig. S5B). A lower IC₅₀ generally indicates a higher potency; thus, ML382 dose-dependently increased the potency of BAM8–22, further demonstrating that ML382 is a PAM of MRGPRX1. The fact that ML382 increased the affinity, but not the maximum response, implies that BAM8–22 is a full agonist. Thus, the allosteric effects on both affinity and efficacy would be translated into apparent affinity in a functional assay. To dissect the ML382 action further, we applied a ternary complex model developed by De Lean et al. (47) to measure its cooperativity factor and binding affinity. Titrating ML382 in the presence of a subsaturating concentration of BAM8–22 is a straightforward approach for establishing this model because ML382 itself does not activate MRGPRX1, but its affinity would change under the influence of BAM8–22 when these two molecules exhibit allostery. The ternary complex model also provides a factor known as α, which can be used as an indicator to quantify the magnitude of this allosteric regulation. We found the IC₅₀ of ML382 to be 3.2 ± 1.7 µM and the α value to be 11.5 ± 1.3. The fact that α was much larger than 1 suggests that ML382 is a potent PAM (*SI Appendix*, Fig. S5C). MRGPRC11 is a mouse ortholog of MRGPRX1 that can also be activated by BAM8–22. However, ML382 did not exert any effect on BAM8–22 inhibition of HVA I_{Ca} in MRGPRC11-expressing DRG neurons (*SI Appendix*, Fig. S5D). Accordingly, ML382 is selective to MRGPRX1.

ML382 Potentiated MRGPRX1-Mediated Inhibition of Synaptic Transmission in Spinal Cord Dorsal Horn Neurons. Because changes in HVA I_{Ca} in the soma of DRG neurons may not reflect changes in their central terminals, we conducted patch-clamp recording of evoked excitatory presynaptic currents (eEPSCs) in dorsal horn neurons, which receive inputs from nociceptive afferent fibers. Unlike in cultured neurons, heterologous expression of MRGPRX1 is not feasible at central terminals of DRG neurons. Even if it were possible, MRGPRX1 may be overexpressed or expressed nonselectively in various subsets of DRG neurons, which would prevent delineation of the physiological role of endogenous MRGPRX1 in modulating spinal synaptic transmission. However, *MrgprX1* mice allow us to continue testing how MRGPRX1 at central terminals of native DRG neurons regulates spinal synaptic transmission.

In *MrgprX1* mice with complete Freund's adjuvant (CFA)-induced hind paw inflammation, we recorded eEPSCs in substantia gelatinosa (SG; lamina II) neurons in lumbar spinal cord slices (L4-L5 segments; Fig. 5*A*). High-intensity paired-pulse stimulation (500 µA, 0.1 ms, 400 ms apart, three tests per minute) was applied at the dorsal root to activate high-threshold afferent fibers (C-fibers) (48). Bath application of 0.5 µM BAM8–22 induced a strong inhibition of first eEPSCs in 10 of 18 SG neurons

(55.6%). Further, the effect of BAM8–22 was significantly enhanced by cotreatment with ML382 (Fig. 5 *B–D*). Importantly, BAM8–22 did not inhibit eEPSCs in any of the SG neurons from *Mrgpr⁻/⁻* mice, in the presence or absence of ML382 (Fig. 5*E*). In addition, ML382 alone did not alter eEPSCs in any experiment (Fig. 5*F*). The paired-pulse ratio (PPR) is defined as the peak amplitude of the second eEPSC (P2) divided by the first eEPSC (P1) evoked by two pulses. The reduction of first eEPSCs by BAM8–22 with ML382 was associated with an increased PPR in *MrgprX1* mice, suggesting presynaptic inhibition of excitatory neurotransmitter release (48, 49). This phenomenon was not observed in *Mrgpr⁻/⁻* mice, and ML382 alone did not affect PPR.
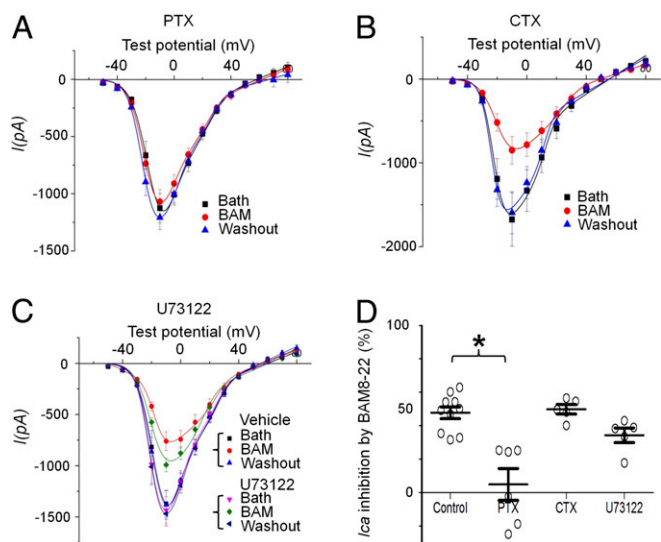

Fig. 3. Inhibition of HVA I_{Ca} by *MrgprX1* agonist depends on the $G_{\alpha i/o}$ pathway. (*A*) Overnight pretreatment of DRG neurons from *MrgprX1* mice with PTX (2 µg/mL, to block $G_{\alpha i/o}$) abolished the inhibition of HVA Ca²⁺ currents (I_{Ca}) by BAM8–22 (BAM, 5 µM). (*B*) Overnight pretreatment with CTX (2 µg/mL, to uncouple $G_{\alpha s}$ functionally) did not affect BAM8–22-induced inhibition. (*C*) Acute perfusion with U73122 (5 µM, 3 min) to inhibit the phospholipase C pathway did not affect BAM8–22-induced inhibition. (*D*) Amplitude of BAM8–22-induced I_{Ca} inhibition in the absence (control) and presence of different blockers, normalized by the pre-BAM8–22 baseline. Controls are presented as a combined group. *$P < 0.05$ vs. respective control, Student *t* test (*n* = 5–6 neurons per group).
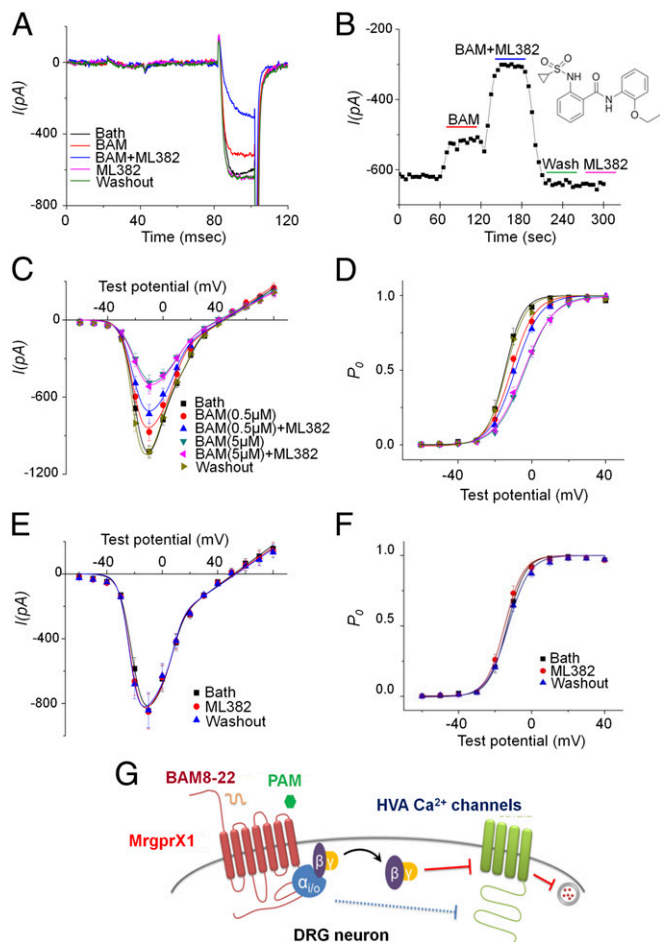
Fig. 4. ML382 enhances BAM8–22 inhibition of HVA I_{Ca} in DRG neurons from *MrgprX1* mice. (*A*) Representative trace shows the protocol used to record current from LVA and HVA Ca²⁺ channels. The inhibition of HVA I_{Ca} by a low dose of BAM8–22 (BAM, 0.5 μM) was significantly enhanced by ML382 (5 μM). However, ML382 alone did not inhibit HVA I_{Ca}. (*B*) Representative time course of the drug effects on HVA I_{Ca}. The enhancement of BAM8–22-induced inhibition of HVA I_{Ca} by ML382 (5 μM) is rapid and reversible. (*Inset*) Chemical structure of ML382. (*C*) I-V relation showing the inhibitory effects of BAM8–22 (0.5 μM and 5 μM) with and without ML382 (5 μM) cotreatment. (*D*) Activation curves show that BAM8–22 shifts the voltage dependency of the activation curve to more positive membrane potentials. P_0, channel open probability. ML382 (5 μM) alone did not inhibit I_{Ca} (*E*) or shift the voltage dependency (*F*). Symbols in *D* are indicated in *C*. (*G*) Schematic model of *MrgprX1*-mediated HVA I_{Ca} inhibition, which is promoted, in part, by $G_{\beta\gamma}$ binding and depends on the $G_{\alpha i/o}$ pathway. ML382 is a selective *MrgprX1* allosteric agonist that can boost BAM8–22-induced current inhibition by increasing its binding affinity (*n* = 6–8 neurons per group).

BAM22 Expression Was Up-Regulated in the Spinal Cord After Injury.

BAM22 is an endogenous peptide that may be secreted in the spinal cord to activate both MRGPRX1 and opioid receptors. BAM22 immunoreactivity was significantly increased in the spinal cord dorsal horn (L4-L5) ipsilateral to the side of hind paw inflammation (2 d after intraplantar injection with CFA) and nerve injury (2 wk after sciatic CCI) in *MrgprX1* mice (Fig. 6*A*). The increase in BAM22 immunoreactivity appeared mostly at the superficial dorsal horn (laminae I-II) on the injured side (50). We validated the specificity of BAM22 antibody by preabsorbing the anti-BAM22 antiserum with 10^{-6} M BAM22, resulting in the complete absence of BAM22 signal (*SI Appendix*, Fig. S6).

Because no *BAM22* knockout mice are available to establish the antibody specificity further, we next quantified the level of BAM22 in mouse spinal cord by using a highly selective targeted

mass spectrometry (MS) approach termed liquid chromatography (LC)-selected reaction monitoring (SRM). The BAM22, together with other molecules, was extracted from the spinal cord, trypsinized, and resolved by reverse-phase LC. The eluted BAM22$_{8–19}$ peptide (VGRPEWWMDYQK) was ionized and transferred into MS that was operated in a mode of SRM. In SRM, the BAM22 peptide ion was separated from other coeluting ions and then fragmented to generate specific product ions, which indicated the intensity of BAM22 in the original samples (Fig. 6*B*). In such a targeted analysis, we first defined the precursor ion and fragmented MS/MS pattern of the BAM22$_{8–19}$ peptide using a synthetic peptide and then measured the absolute level of BAM22 peptide in CFA-treated spinal cord (247 ± 2 fmol per spinal cord, 6.8 nM; Fig. 6*C*). Whereas BAM22 was quantified by three different product ions, the specificity of this analysis was strongly supported by identical features between the endogenous BAM22-derived peptide and its synthetic counterpart, with respect to precursor ion, LC retention time, and multiple product ions. Finally, based on five product ions, we found that CFA treatment induced a significant increase (46.0 ± 3.6%) in the spinal cord BAM22 level (Fig. 6*D*). Thus, LC-SRM unambiguously demonstrated an up-regulation of BAM22 in the spinal cord after injury. The level of BAM22 in skin was undetectable in both the control and CFA-treated mice.

ML382 Inhibited Evoked Pain Hypersensitivity After Injury in an MRGPRX1-Dependent Manner.

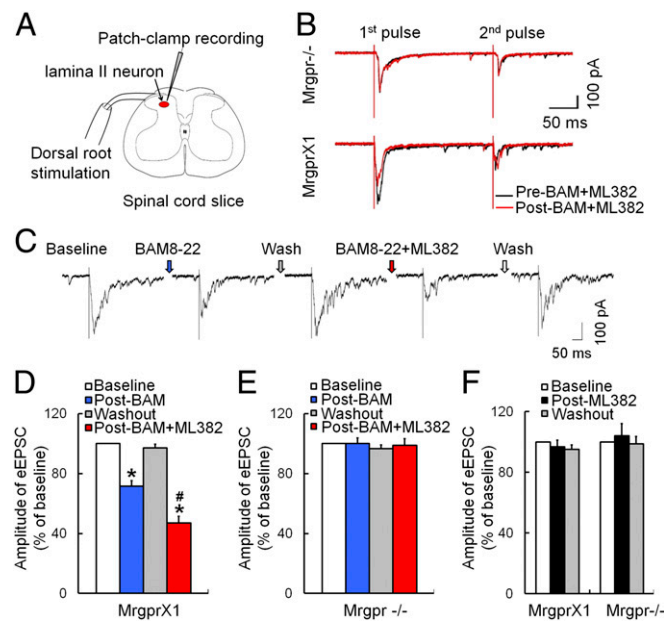Our findings suggest that MRGPRX1 and its endogenous orthosteric agonist BAM22 may function at the central

Fig. 5. ML382 enhances the inhibition of spinal synaptic transmission by BAM8–22 in *MrgprX1* mice. (*A*) Experimental setup of patch-clamp recording from SG neurons in a spinal cord slice. The high-intensity test stimulation (500 μA, 0.1 ms) was applied to the dorsal root. (*B*) Representative traces of eEPSCs to high-intensity, paired-pulse stimulation (500 μA, 0.1 ms, 400-ms interval) before (black) and 5 min after (red) bath application of BAM8–22 (BAM, 0.5 μM) and ML382 (5 μM) in SG neurons from *MrgprX1* mice and *Mrgpr⁻/⁻* mice. (*C*) Representative trace of eEPSCs to high-threshold afferent inputs before and after drug treatment in *MrgprX1* mice. (*D*) BAM8–22 (0.5 μM) significantly decreased eEPSCs of SG neurons in CFA-treated *MrgprX1* mice (*n* = 10). The inhibition was enhanced by ML382 (5 μM, *n* = 10 neurons). *$P < 0.05$ vs. baseline, #$P < 0.05$ vs. BAM8–2; one-way repeated-measures ANOVA with a Bonferroni post hoc test. (*E*) SG neurons from *Mrgpr⁻/⁻* mice did not respond to BAM8–22 or ML382 (*n* = 8). (*F*) ML382 (5 μM) alone did not affect eEPSCs in SG neurons from *MrgprX1* mice (*n* = 7) or *Mrgpr⁻/⁻* mice (*n* = 11).
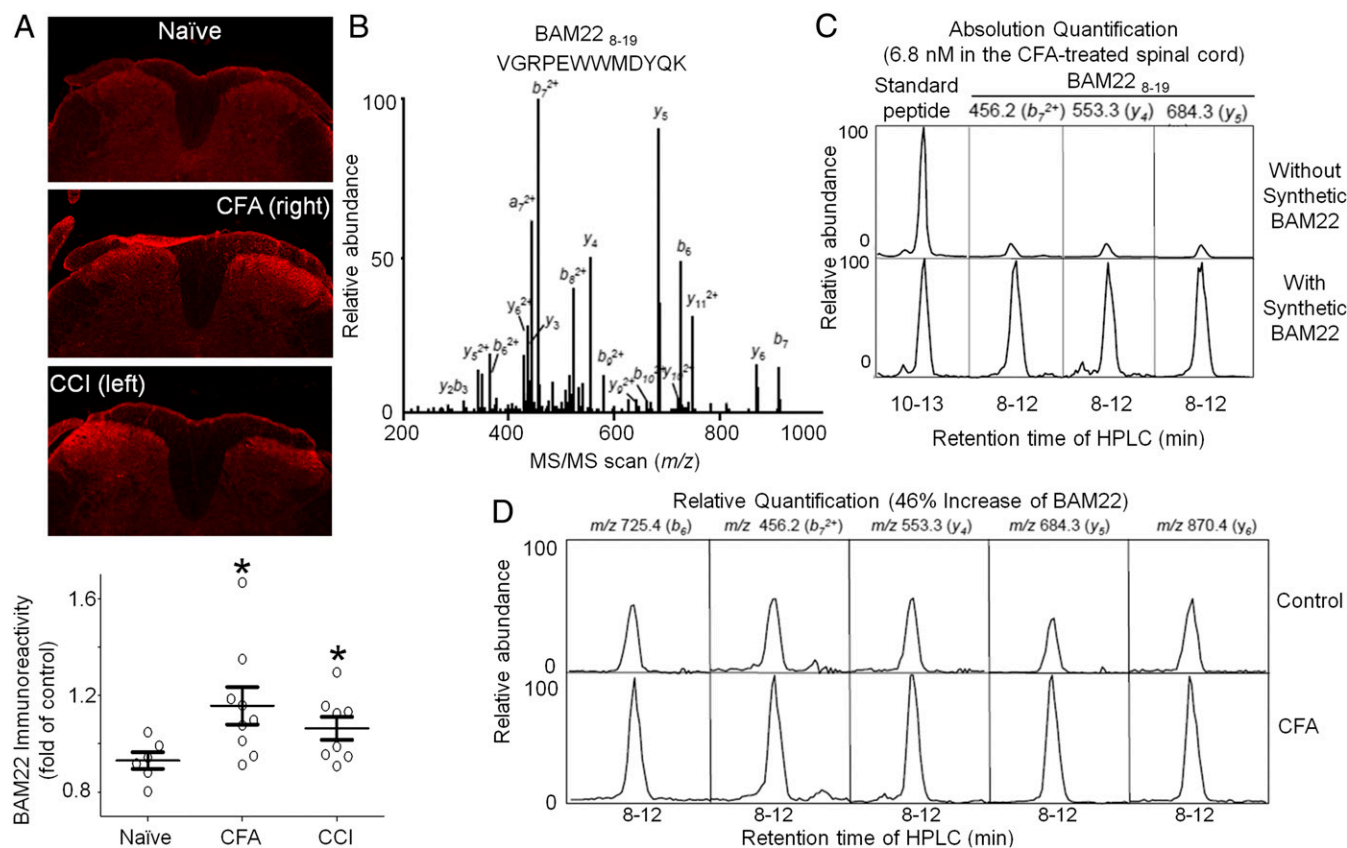
Fig. 6. Level of BAM22 increases in the spinal cord after injury. (*A, Upper*) Representative staining of L4-L5 spinal cord dorsal horn from naive wild-type mice, mice at 2 d after intraplantar injection of CFA, and mice at 2 wk after CCI of the sciatic nerve. (*A, Lower*) Quantification of BAM22 immunoreactivity. *$P < 0.05$ vs. naive ($n = 5$–6 repetitions), one-way ANOVA. (*B*) MS/MS spectrum of triply charged BAM22$_{8-19}$ tryptic peptide (VGRPEWWMDYQK, 532.3 m/z). (*C*) Absolute quantitative analysis of BAM22$_{8-19}$ (6.8 nM) in the CFA-treated mouse spinal cord by LC-SRM, based on peak area difference in the CFA-treated spinal cord samples before and after addition of 250 fmol of synthetic BAM22. Three product ions were monitored. In addition, the run-to-run variation was corrected by spiking in 100 fmol of another synthetic peptide (TLSDYNIQKESTLHLVLR, triply charged precursor ion of 710.8 m/z) as an external standard. (*D*) Comparison of the BAM22 expression level between control and CFA-treated mouse spinal cords shows that CFA induced an increase ($46.0 \pm 3.6\%$) in BAM22 level. Five transitions were monitored for relative quantification.

terminals of DRG neurons. Therefore, we next examined if ML382 by itself attenuates persistent pain in vivo. ML382 was i.th. applied (25 μM, 5 μL) half an hour before formalin [2% (vol/vol) formaldehyde, 5 μL] was injected into the plantar aspect of one hind paw. The first phase of pain response (0–10 min postformalin) was not affected, but the later phase of inflammatory pain response (10–60 min postformalin) was significantly attenuated by ML382 in *MrgprX1* mice compared with *Mrgpr*$^{-/-}$ mice (Fig. 7 *A* and *B*). In models of CFA-induced inflammatory pain (Fig. 7 *C* and *D*) and sciatic CCI-induced neuropathic pain (Fig. 7 *E* and *F*), ML382 (25 μM, 125 μM, and 250 μM; 5 μL; i.th. administration) dose-dependently attenuated heat hypersensitivity in *MrgprX1* mice, but not in *Mrgpr*$^{-/-}$ mice. Contralateral heat nociception was not affected by drug treatment. Therefore, ML382 was able to induce antihyperalgesic effects without requiring exogenous BAM peptides.

To quantify the concentration of ML382 exposed at the spinal cord, we dissected the spinal cords out 30 min after i.th. injection of ML382 (10 μL of 250 μM) or saline (10 μL) as a control and incubated the spinal cord in 500 μL of oxygen-saturated artificial cerebral spinal fluid (aCSF) at 37 °C for 1 h. The amount of ML382 in the aCSF was detected using LC/MS analysis. The amount of ML382 detected was 4.48 ± 2.24 ng/mL (average $\pm$ SEM; $n = 3$). Assuming the drug is diluted 50-fold in the aCSF (because the amount of endogenous cerebral spinal fluid is minimal), the concentration was 1.08 ± 0.68 μM. The actual concentration at the lumbar region in vivo could be higher because the i.th. injection is between lumbar 5 and sacral 1. The

amount of ML382 in saline-injected mice was below the limit of quantification. We also measured the level of ML382 over time in plasma and found that it is relatively stable in human and rat plasma, but not in mouse plasma (*SI Appendix*, Table S1).

ML382 Inhibited Nerve Injury-Induced Ongoing Pain in *MrgprX1* Mice.
In *MrgprX1* mice that had undergone CCI, lumbar puncture injection of ML382 alone (25 μM, 5 μL) led to a significant increase in postconditioning time spent in the ML382-paired chamber, compared with the preconditioning value (Fig. 8*A*). Simultaneously, the mice decreased time spent in the vehicle (saline)-paired chamber. However, *Mrgpr*$^{-/-}$ mice showed no significant change in postconditioning time spent in the ML382- or vehicle-paired chamber, compared with the respective preconditioning values (Fig. 8*A*; $n = 10$ per group). The difference score showed that only *MrgprX1* mice had a preference for the ML382-paired chamber (Fig. 8*B*). These results suggest that ML382 itself can alleviate ongoing pain after nerve injury in *MrgprX1* mice, presumably by enhancing the pain inhibition from a sufficient supply of endogenous orthosteric ligands (e.g., BAM22) in the spinal cord, as suggested by HPLC data (Fig. 6). Importantly, ML382 did not induce CPP in sham-operated animals of either genotype, suggesting that CPP results from pain relief in *MrgprX1* mice and that the drug itself does not activate innate reward circuitry in the absence of pain (Fig. 8 *C* and *D*; $n = 9$ per group). ML382 at a much higher dose (250 μM, 5 μL,
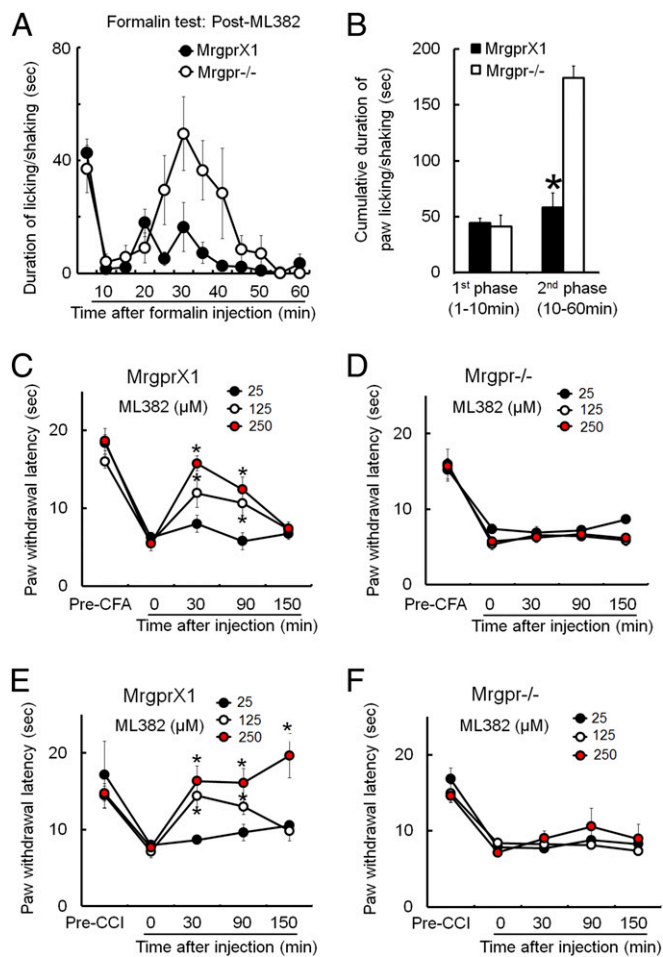
Fig. 7. ML382 alone attenuated evoked pain hypersensitivity in *MrgprX1* mice without exogenous BAM8–22. (*A*) Time course of pain behavior elicited by intraplantar injection of formalin [2% (vol/vol), 5 µL] into *MrgprX1* and *Mrgpr*$^{-/-}$ mice that had been pretreated with i.th. ML382 (25 µM, 5 µL, 15 min). (*B*) Cumulative duration of paw licking and shaking after formalin injection showed that the second phase of pain behavior was significantly reduced by ML382 in *MrgprX1* mice (*n* = 8 per group). *$P < 0.05$ vs. *Mrgpr*$^{-/-}$, Student *t* test. (*C*) PWL to noxious heat stimuli was measured with the Hargreaves test. Heat hypersensitivity in the ipsilateral hind paw at day 2 after intraplantar injection of CFA was dose-dependently attenuated by i.th. ML382 in *MrgprX1* mice (*n* = 5–7 per dose). *$P < 0.05$ vs. predrug, two-way mixed-model ANOVA with a Bonferroni post hoc test. (*D*) However, ML382 was not effective in *Mrgpr*$^{-/-}$ mice (*n* = 5–7 per dose). (*E* and *F*) CCI of sciatic nerve-induced heat hypersensitivity of the ipsilateral hind paw. The hypersensitivity was dose-dependently attenuated by ML382 in *MrgprX1* mice (*E*), but not in *Mrgpr*$^{-/-}$ mice (*F*) (*n* = 5–7 per dose). *$P < 0.05$ vs. predrug, two-way mixed-model ANOVA with a Bonferroni post hoc test.

i.th. administration) did not affect locomotor function in either genotype (Fig. 8*E*; *n* = 7).

Besides inhibiting pain, MRGPRX1 may also function as an itch receptor in the peripheral nerve terminals (15, 18). We scored mice for scratching behavior at 0–30 min after drug injection. As previously reported, s.c.-injected BAM8–22 induced a significant increase in scratching behavior compared with saline (13, 15, 18) (Fig. 8*F*). However, ML382 did not induce significant scratching when injected s.c. into the back or by i.p. or i.th. injection. These findings indicate that ML382 does not induce itch at these sites (Fig. 8*F*; *n* = 5–6 per group).

Discussion

Most analgesics available for chronic pain treatment have severe side effects because their targets exist both inside and outside the

pain pathway and are widely distributed in the CNS (1–4). Using *MrgprX1* transgenic mice, we showed that both a full agonist (BAM8–22) and PAM (ML382) of MRGPRX1 alleviate persistent pain, including ongoing pain after nerve injury, and revealed the underlying cellular mechanisms. Further, we provide evidence that ML382 allosterically enhances BAM8–22-induced inhibition of HVA I_{Ca} in native DRG neurons and augments the suppression of eEPSCs to high-threshold afferent inputs in lamina II dorsal horn neurons. The pain inhibition by BAM8–22 and ML382 was MRGPRX1-dependent and presumably followed a reduction in calcium-dependent neurotransmitter release from central terminals of primary sensory neurons.

The full-length BAM22 peptide is a potent ligand for MRGPRX1 and MRGPRC, with the C-terminal 15 amino acids activating these receptors (10, 23, 24). It also contains the characteristic
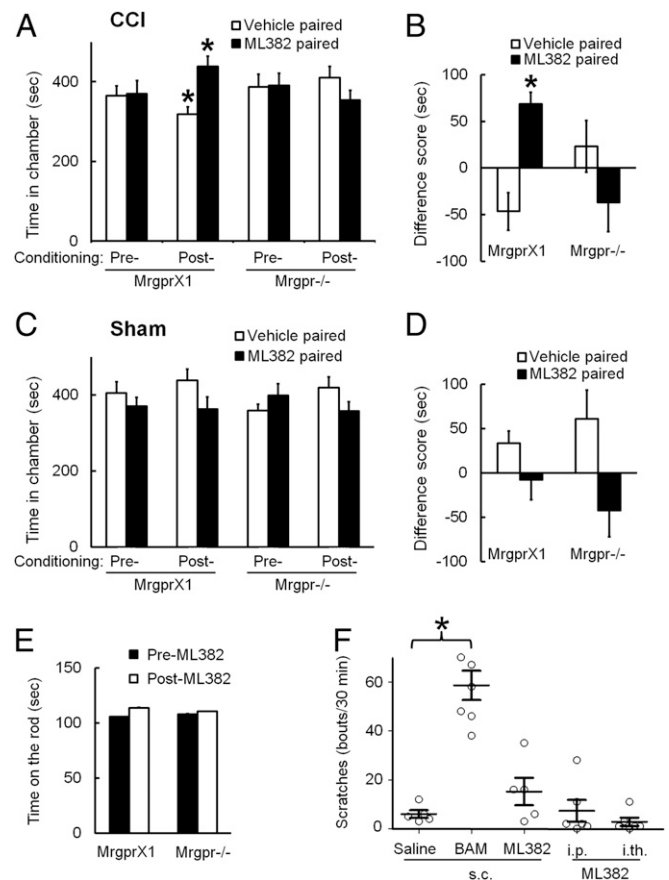

Fig. 8. I.th. administration of ML382 alone induces CPP in *MrgprX1* mice after nerve injury. (*A*) *MrgprX1* mice at day 7–13 post-CCI spent more time in the chamber paired with ML382 (25 µM, 5 µL, i.th.), and less time in the vehicle-paired chamber, after conditioning treatment. ML382 did not induce CPP in *Mrgpr*$^{-/-}$ mice after CCI (*n* = 10 per group). *$P < 0.05$ vs. preconditioning (details on the experimental time line are provided in *Methods*), two-way repeated measures ANOVA with a Bonferroni post hoc test. (*B*) Difference scores [(Postconditioning time) − (Preconditioning time)] in the ML382-paired chamber were significantly greater than difference scores in the vehicle-paired chambers for *MrgprX1* mice. *$P < 0.05$ vs. vehicle, paired *t* test. (*C* and *D*) ML382 did not induce CPP in *MrgprX1* or *Mrgpr*$^{-/-}$ mice that received sham surgery (*n* = 9 per group). Two-way repeated measures ANOVA, with a Bonferroni post hoc test, $P > 0.05$. (*E*) I.th. injection of ML382 at a higher dose (250 µM, 5 µL) did not impair motor function of *MrgprX1* or *Mrgpr*$^{-/-}$ mice in the rota-rod test at 30–60 min postinjection (*n* = 7 per group). (*F*) ML382 did not cause itch in *MrgprX1* mice when applied s.c. (1.0 mM, 5 µL) into the back, i.p. (5 mM, 10 µL), or i.th. (25 µM, 5 µL). In contrast, s.c. injection of BAM8–22 (BAM; 1.0 mM, 5 µL) caused rigorous scratching behavior (*n* = 5–6 per group). *$P < 0.05$, one-way ANOVA with a Bonferroni post hoc test.

Met-enkephalin YGGFM motif at the N terminus that can activate classic opioid receptor subtypes (μ, δ) (23). However, this motif is dispensable for the MRGPR activity. MRGPRX1 is also insensitive to the classical opioid receptor antagonists and showed distinct structure–activity relationships and pharmacology with its known ligands. The level of BAM22 is up-regulated in the spinal cord of *MrgprX1* mice after tissue inflammation and nerve injury. Up-regulation of BAM22 and MRGPRC receptor has also been reported in rodent models of inflammatory and neuropathic pain (14, 51, 52). Accordingly, enhanced endogenous pain inhibition mediated by MRGPRC and MRGPRX1 in rodents and humans may parallel endogenous pain inhibition of opioid receptors and converge on BAM peptide to suppress chronic pain (53, 54). The finding that ML382 can inhibit pain after injury without exogenous BAM peptide further supports this notion.

N-type HVA calcium channels play an important role in controlling the release of neurotransmitter vesicles from central terminals of nociceptive DRG neurons into spinal cord (33, 34, 36, 37, 55). Accordingly, N-type channels have been important targets for the development of drugs to treat pain (33, 34, 56). However, because these channels are broadly expressed throughout the peripheral nervous system and CNS, channel blockers pose side effects, such as nausea, anxiety, and sweating (57–59). BAM8–22 mainly inhibits N-type channels in DRG neurons from *MrgprX1* mice, similar to what we found with MRGPRC activation (48). Whereas the activation of MRGPRC leads to inhibition of HVA I_{Ca} through a phospholipase C-dependent mechanism, our findings suggest that MRGPRX1 inhibition of HVA I_{Ca} is mainly mediated by $G_{i/o}$-sensitive $G\beta\gamma$ binding and may also involve a $G\beta\gamma$-independent pathway. N-type channels are also an important target for opioid inhibition of pain through the $G_{i/o}$ pathway (39, 60–62), indicating again that MRGPRX1 may be another endogenous inhibitory mechanism parallel to the endogenous inhibitory mechanism of opioids. Importantly, MRGPRX1 is restricted to the pain pathway and may selectively modulate HVA calcium channels in primary nociceptive neurons to attenuate persistent pain. Therefore, full agonists and PAMs to MRGPRX1, rather than direct Ca^{2+} channel blockers, likely attenuate persistent pain while avoiding central and peripheral side effects.

ML382 did not enhance the inhibition of HVA I_{Ca} by BAM8–22 in MRGPRC11-expressing DRG neurons from wild-type mice. MRGPRX1 and MRGPRC11 exhibit considerably different drug profiles even though they share 54% amino acid identity (24). Species differences across MRGPRs are the main reason why many agonists have been reported for MRGPRX1 but only a few could be tested for in vivo functions (10, 18, 28). Thus, our *MrgprX1* mice provide a unique rodent platform to screen compounds against the human MRGPRX1 and test their functions in vivo.

In *Mrgpr*$^{-/-}$ mice, 30 Mrgprs were knocked out, 12 of which have intact ORFs. The peptide BAM8–22 is a specific ligand of mouse MRGPRC11, rat MRGPRC, and MRGPRX1. More importantly, BAM8–22 does not activate any other Mrgprs. We have shown that DRG neurons of *Mrgpr*$^{-/-}$ mice did not respond to BAM8–22 and specific knockdown *MrgprC11* in wild-type DRG neurons also eliminated BAM8–22-induced activation (15). Because the *MrgprC11* locus has an extremely high level of repetitive sequences, multiple attempts by homologous recombination and CRISPR approaches to generate *MrgprC11* single-gene knockout mice have failed. The *Mrgpr*$^{-/-}$ mice are still the best option to study *MrgprC11* in vivo, along with substitution of the human *MrgprX1*. However, the limitation of *Mrgpr*$^{-/-}$ mice is potential gene compensation from other *Mrgprs*.

Both BAM8–22 and ML382 alleviated evoked pain hypersensitivity in *MrgprX1* mice, but not in *Mrgpr*$^{-/-}$ mice, after tissue inflammation and nerve injury. Importantly, both drugs produced CPP in *MrgprX1* mice after sciatic CCI, indicating the relief of ongoing neuropathic pain. Operant behavior studies,

such as CPP, measure the affective aspect of the spontaneous pain experience, which relates closely to the complex human experience of chronic pain (63, 64). Therefore, the findings from this operant behavior study have translational relevance and indicate that agonists and PAMs of MRGPRX1 are promising new antihyperalgesic compounds. BAM8–22 and ML382 did not induce CPP in sham-operated animals, suggesting that they are not rewarding in the absence of ongoing pain and have a low likelihood for addiction and abuse.

One limitation of ML382 is that it did not inhibit mechanical allodynia induced by sciatic nerve CCI in *MrgprX1* mice (*SI Appendix*, Fig. S7). However, BAM8–22 and its analog, JHU58, were reported to attenuate mechanical allodynia as well as thermal hyperalgesia and neuropathic pain in wild-type mice and rats (6, 21). A possible explanation for the discrepancy is that the *MrgprX1* expression level in *MrgprX1* transgenic mice is not as high as rodent MrgprC expression such that the activation of MRGPRX1 cannot exert the antimechanical allodynia effect.

Allosteric ligands that bind at allosteric binding sites provide better temporal and spatial specificity control of endogenous physiological signaling than orthosteric ligands alone because they require colocalization of the receptor and endogenous orthosteric ligand to function. Directly activating MRGPRX1 at peripheral terminals may induce itch (15, 18); therefore, activation of peripheral MRGPRX1 with an orthosteric ligand is not a viable approach to pain relief. Intriguingly, during chronic pain conditions, the BAM22 level is up-regulated in the superficial dorsal horn, which contains central terminals of nociceptive sensory neurons. However, its level is below the limit of detection in the skin. Thus, i.th. ML382 would specifically maximize the suppression of spinal nociceptive transmission by endogenous BAM22. Indeed, persistent pain was inhibited only when ML382 were administered by the i.th. route, not the i.p. route (*SI Appendix*, Fig. S8). The lack of inhibitory effect on pain by i.p. injection of ML382 is likely due to a combination of lower blood–brain barrier (BBB) penetration and possibly high protein binding of the compound. Nevertheless, i.th. injection of ML382 (0.25 mM, 5 µL) exerted a similar level of pain inhibition as morphine at a higher molar dose (1.0 mM, 5 µL; comparing Fig. 7*E* and *SI Appendix*, Fig. S9). Further modification to the structure of ML382 is ongoing to improve its penetration of the BBB and enable future systemic administration.

In summary, the *MrgprX1* mouse line is a promising model for screening MRGPRX1 ligands and testing their functions at both cellular and systemic levels. MRGPRX1 ligands may be pain-specific inhibitors because the receptors are expressed mostly in primary sensory neurons and modulate nociceptive transmission (7–11). Further, both MRGPRX1 full agonists and PAMs may improve selectivity of pain inhibition, and hence are potential new classes of drugs to treat persistent pain conditions.

Methods

All animal experiments were performed under protocols approved by the Animal Care and Use Committee of the Johns Hopkins University School of Medicine.

Generation of *MrgprX1* Mice. We purchased a mouse BAC clone (RP23-311C15) containing the entire *Mrgpra3* gene from the Children's Hospital Oakland Research Institute. We modified the BAC clone using homologous recombination in bacteria to generate the *MrgprC11*^{MrgprX1} mouse line. We crossed these mice with *MrgprA3*$^{GFP-Cre}$ (13) and *Mrgpr-cluster*$\Delta^{-/-}$ (15) lines that we had generated previously. We used the *MrgprC11*^{MrgprX1} transgenic line and *MrgprA3*$^{GFP-Cre}$ transgenic line as hemizygotes or heterozygotes for all experiments.

Chronic Pain Models. Inflammation was induced by injecting the hind paw of mice s.c. with 5 µL of 50% (vol/vol) CFA solution in saline (21). Pain response change was evaluated 24–48 h after injection.

Neuropathic pain was induced by CCI of the sciatic nerve as previously described (6). Mice were anesthetized by inhalation of 2% (vol/vol) isoflurane delivered

through a nose cone. The left sciatic nerve at the middle thigh level was separated from the surrounding tissue and loosely tied with three nylon sutures (9-0 nonabsorbable monofilament; S&T AG). The ligatures were ∼0.5 mm apart.

Behavioral Studies. Behavioral assays were performed by experimenters blinded to genotype. The mice used in the tests were backcrossed to C57BL/6 mice for at least 10 generations and were 2- to 3-mo-old males (weighing 20–30 g).

I.th. injection was performed as previously described (21). Briefly, ML382 was dissolved in DMSO to 50 mM, suspended in 0.9% saline to the desired working concentration, and injected into the i.th. space under brief isoflurane (1.5%) anesthesia. A 30-gauge, 0.5-inch needle connected to a 50-μL syringe was inserted into one side of the L5 or L6 spinous process and moved carefully forward to the intervertebral space. A tail flick indicated that the tip of the needle was inserted into the subarachnoid space. The needle was removed after 5 μL of drug solution was administered.

One day before the formalin test, mice were acclimated to the environment for 1 h. On the day of test, 5 μL of 2% (vol/vol) formalin in saline was injected into the plantar region of one hind paw. Spontaneous pain behavior (licking and shaking) was recorded for 60 min (21).

The Hargreaves test was performed as previously described (13). Mice were placed under a transparent plastic box (4.5 × 5 × 10 cm) on a glass floor. Infrared light was delivered through the glass floor to the hind paw. After acclimatization sessions, the latency for the animal to withdraw its hind paw was measured.

For the CPP test, humanized *MrgprX1* and *Mrgpr⁻/⁻* mice underwent CCI of the left sciatic nerve. On day 7 after CCI, both naive and nerve-injured animals were habituated (30 min·d⁻¹) in an automated three-chamber box in which they had access to all chambers. The two larger chambers of this apparatus contained distinct visual (vertical stripes vs. triangular shapes) and tactile (smooth floor vs. grooved floor) cues. The third, smaller chamber was interposed between the other two and was devoid of overt spatial cues. On the preconditioning day (day 11 post-CCI), behavior was video-recorded for 15 min while the mice were again free to explore all three chambers. The results were used to quantify any basal chamber preference or aversion in individual mice. In keeping with a previous study (32), animals that spent more than 80% (>720 s) or less than 20% (<120 s) of the total time in any given chamber were eliminated from further testing. The next day (day 12 post-CCI), animals received a lumbar puncture injection of vehicle (5 μL of saline) under anesthesia 10 min before being placed in one of the conditioning chambers for 45 min. Four hours later, the same animals received a lumbar puncture injection of ML382 (250 μM, 5 μL), and 10 min later, they were restricted to the opposite conditioning chamber for 45 min. On the postconditioning test day (day 13 post-CCI), animals were placed in the same three-chamber box with access to all chambers but received no injection. Their behavior was recorded for 15 min and used to analyze chamber preference or aversion. Data were pooled from seven groups of mice, each containing nerve-injured and naive animals of both genotypes (*MrgprX1* and *Mrgpr⁻/⁻*). Pairing of ML382 or vehicle with a given chamber was counterbalanced between groups. For each treatment group, we compared time spent in each chamber during pre- and postconditioning days by paired *t* test to determine if conditioned place aversion or preference was present. An increase in postconditioning time spent in the ML382-paired chamber, compared with preconditioning time in the same chamber, indicated CPP. In addition, difference scores were calculated as follows: (Postconditioning time − Preconditioning time).

Cell Culture. DRGs from 3- to 4-wk-old mice were collected in cold DH10 medium [DMEM/F-12 with 10% (vol/vol) FBS and 1% penicillin/streptomycin; Gibco] and treated with enzyme solution (5 mg/mL dispase and 1 mg/mL collagenase type I in HBSS without Ca²⁺ and Mg²⁺; Gibco) at 37 °C. After trituration and centrifugation, cells were resuspended in DH10 with nerve growth factor (50 ng/mL; Upstate Biotechnology) and glial cell line-derived neurotrophic factor (25 ng/mL; R&D Systems), plated on glass coverslips

coated with poly-ᴅ-lysine (100 μg/mL; Biomedical Technologies) and laminin (10 μg/mL; Invitrogen), cultured at 37 °C, and used after 20–40 h (15).

Whole-Cell Recordings of Cultured DRG Neurons. Whole-cell currents of cultured DRG neurons with *MrgprA3*-GFP marker were recorded with an Axon 700B amplifier and pCLAMP 9.2 software (Molecular Devices). Extracellular solution contained 130 mM *N*-methyl-ᴅ-glucamine chloride (NMDG-Cl), 5 mM BaCl₂, 1 mM MgCl₂, 10 mM Hepes, and 10 mM glucose, with pH of 7.4 adjusted with 1 M NMDG. Osmolality was adjusted to 310 mOsm/kg with sucrose. Electrodes were pulled (Model pp-830; Narishige) from borosilicate glass (World Precision Instruments) with resistances of 2–4 MΩ. Pipette solution contained 140 mM tetraethylammonium chloride, 10 mM EGTA, 1 mM MgCl₂, 10 mM Hepes, 0.5 mM GTP, and 3 mM ATP, with pH of 7.4 and osmolality of ∼300 mOsm/kg. The voltage protocol was modified from a previously published method (26). Briefly, cells were held at −80 mV and evoked to −40 mV for 20 ms to activate LVA Ca²⁺ channels, and then held to −60 mV for 20 ms and evoked to −10 mV for 40 ms to activate HVA Ca²⁺ channels. Leak currents were subtracted with the P/4 protocol in pCLAMP 9.2 software. Liquid junction potentials and whole-cell capacitances were offset, and series resistances were compensated by 70%. All experiments were performed at room temperature (2–23 °C).

Downstream Pathway Analysis Using Electrophysiological Recording. We measured the current–voltage relation (I-V curve) by plotting peak currents to the testing voltages, which were then fitted by the double Boltzmann I-V equation

$$I(V) = \frac{(V - Vrev) * Gmax1}{1 + e^{\frac{V - Vhalf1}{k}}} + \frac{(V - Vrev) * Gmax2}{1 + e^{\frac{V - Vhalf2}{k}}}.$$

$I(V)$ is ionic current as the function of membrane voltage, V_{rev} is reversal potential, G_{max} is maximum conductance, V_{half} is the voltage at half-maximum current, and k is a default slope factor.

We measured the voltage dependency of channel activation (P-V curve) by plotting normalized tail currents as the function of testing voltages and then fitting by the Boltzmann equation

$$P(V) = Pmin + \frac{Pmax - Pmin}{1 + e^{\frac{V - Vhalf}{k}}}.$$

$P(V)$ is channel open probability as the function of membrane voltage. P_{min} and P_{max} indicate the minimum and maximum open probability, respectively.

Statistics. Data are presented as mean ± SEM. Groups were compared by a two-tailed, unpaired, or paired Student's *t* test, or by a one-way repeated-measures ANOVA test or two-way ANOVA test followed by Bonferroni post hoc comparisons according to experimental design. $P < 0.05$ was considered a statistically significant difference. Experiments were replicated biologically at least three times.

1. Breivik H, Collett B, Ventafridda V, Cohen R, Gallacher D (2006) Survey of chronic pain in Europe: Prevalence, impact on daily life, and treatment. *Eur J Pain* 10(4):287–333.
2. Portenoy RK (1996) Opioid therapy for chronic nonmalignant pain: A review of the critical issues. *J Pain Symptom Manage* 11(4):203–217.
3. Scholz J, Woolf CJ (2002) Can we conquer pain? *Nat Neurosci* 5(Suppl):1062–1067.
4. Pope JE, Deer TR, Kramer J (2013) A systematic review: Current and future directions of dorsal root ganglion therapeutics to treat chronic pain. *Pain Med* 14(10):1477–1496.
5. Basbaum AI, Bautista DM, Scherrer G, Julius D (2009) Cellular and molecular mechanisms of pain. *Cell* 139(2):267–284.
6. He SQ, et al. (2014) MrgC agonism at central terminals of primary sensory neurons inhibits neuropathic pain. *Pain* 155(3):534–544.
7. Dong X, Han S, Zylka MJ, Simon MI, Anderson DJ (2001) A diverse family of GPCRs expressed in specific subsets of nociceptive sensory neurons. *Cell* 106(5):619–632.
8. Zhang L, et al. (2005) Cloning and expression of MRG receptors in macaque, mouse, and human. *Brain Res Mol Brain Res* 133(2):187–197.
9. Gloriam DE, Fredriksson R, Schiöth HB (2007) The G protein-coupled receptor subset of the rat genome. *BMC Genomics* 8:338.
10. Lembo PM, et al. (2002) Proenkephalin A gene products activate a new family of sensory neuron–specific GPCRs. *Nat Neurosci* 5(3):201–209.
11. Choi SS, Lahn BT (2003) Adaptive evolution of MRG, a neuron-specific gene family implicated in nociception. *Genome Res* 13(10):2252–2259.
12. Guan Y, Yuan F, Carteret AF, Raja SN (2010) A partial L5 spinal nerve ligation induces a limited prolongation of mechanical allodynia in rats: an efficient model for studying mechanisms of neuropathic pain. *Neurosci Lett* 471(1):43–47.
13. Han L, et al. (2013) A subpopulation of nociceptors specifically linked to itch. *Nat Neurosci* 16(2):174–182.
14. He SQ, et al. (2014) Temporal changes in MrgC expression after spinal nerve injury. *Neuroscience* 261:43–51.
15. Liu Q, et al. (2009) Sensory neuron-specific GPCR Mrgprs are itch receptors mediating chloroquine-induced pruritus. *Cell* 139(7):1353–1365.

16. Liu Q, et al. (2012) Mechanisms of itch evoked by β-alanine. *J Neurosci* 32(42): 14532–14537.

17. Zylka MJ, Dong X, Southwell AL, Anderson DJ (2003) Atypical expansion in mice of the sensory neuron-specific Mrg G protein-coupled receptor family. *Proc Natl Acad Sci USA* 100(17):10043–10048.

18. Sikand P, Dong X, LaMotte RH (2011) BAM8-22 peptide produces itch and nociceptive sensations in humans independent of histamine release. *J Neurosci* 31(20):7563–7567.

19. Flegel C, et al. (2015) RNA-Seq analysis of human trigeminal and dorsal root ganglia with a focus on chemoreceptors. *PLoS One* 10(6):e0128951.

20. Li Z, et al. (2015) The inhibition of high-voltage-activated calcium current by activation of MrgC11 involves phospholipase C-dependent mechanisms. *Neuroscience* 300: 393–403.

21. Guan Y, et al. (2010) Mas-related G-protein-coupled receptors inhibit pathological pain in mice. *Proc Natl Acad Sci USA* 107(36):15933–15938.

22. Schmidt R, Butterworth J, O'Donnell D, Santhakumar V, Tomaszewski M (2009) Cyclic dimers of C-terminal gamma2-MSH analogs as selective antagonists of the human sensory nerve-specific receptor (SNSR-4). *Adv Exp Med Biol* 611:111–112.

23. Mizuno K, Minamino N, Kangawa K, Matsuo H (1980) A new family of endogenous "big" Met-enkephalins from bovine adrenal medulla: Purification and structure of docosa- (BAM-22P) and eicosapeptide (BAM-20P) with very potent opiate activity. *Biochem Biophys Res Commun* 97(4):1283–1290.

24. Han SK, et al. (2002) Orphan G protein-coupled receptors MrgA1 and MrgC11 are distinctively activated by RF-amide-related peptides through the Galpha q/11 pathway. *Proc Natl Acad Sci USA* 99(23):14740–14745.

25. Kunapuli P, et al. (2006) Identification of small molecule antagonists of the human mas-related gene-X1 receptor. *Anal Biochem* 351(1):50–61.

26. Chen H, Ikeda SR (2004) Modulation of ion channels and synaptic transmission by a human sensory neuron-specific G-protein-coupled receptor, SNSR4/mrgX1, heterologously expressed in cultured rat neurons. *J Neurosci* 24(21):5044–5053.

27. Solinski HJ, Boekhoff I, Bouvier M, Gudermann T, Breit A (2010) Sensory neuron-specific MAS-related gene-X1 receptors resist agonist-promoted endocytosis. *Mol Pharmacol* 78(2):249–259.

28. Wen W, et al. (2015) Discovery and characterization of 2-(cyclopropanesulfonamido)-N-(2-ethoxyphenyl)benzamide, ML382: A potent and selective positive allosteric modulator of MrgX1. *ChemMedChem* 10(1):57–61.

29. Conn PJ, Christopoulos A, Lindsley CW (2009) Allosteric modulators of GPCRs: A novel approach for the treatment of CNS disorders. *Nat Rev Drug Discov* 8(1):41–54.

30. Burstein ES, et al. (2006) Characterization of the Mas-related gene family: Structural and functional conservation of human and rhesus MrgX receptors. *Br J Pharmacol* 147(1):73–82.

31. Bennett GJ (2012) What is spontaneous pain and who has it? *J Pain* 13(10):921–929.

32. King T, et al. (2009) Unmasking the tonic-aversive state in neuropathic pain. *Nat Neurosci* 12(11):1364–1366.

33. Gribkoff VK (2006) The role of voltage-gated calcium channels in pain and nociception. *Semin Cell Dev Biol* 17(5):555–564.

34. McGivern JG, McDonough SI (2004) Voltage-gated calcium channels as targets for the treatment of chronic pain. *Curr Drug Targets CNS Neurol Disord* 3(6):457–478.

35. Fox AP, Nowycky MC, Tsien RW (1987) Kinetic and pharmacological properties distinguishing three types of calcium currents in chick sensory neurones. *J Physiol* 394: 149–172.

36. Yusaf SP, Goodman J, Pinnock RD, Dixon AK, Lee K (2001) Expression of voltage-gated calcium channel subunits in rat dorsal root ganglion neurons. *Neurosci Lett* 311(2): 137–141.

37. Catterall WA (2000) Structure and regulation of voltage-gated Ca2+ channels. *Annu Rev Cell Dev Biol* 16:521–555.

38. Bourinet E, et al. (2014) Calcium-permeable ion channels in pain signaling. *Physiol Rev* 94(1):81–140.

39. Moises HC, Rusin KI, Macdonald RL (1994) mu-Opioid receptor-mediated reduction of neuronal calcium current occurs via a G(o)-type GTP-binding protein. *J Neurosci* 14(6): 3842–3851.

40. Macdonald RL, Werz MA (1986) Dynorphin A decreases voltage-dependent calcium conductance of mouse dorsal root ganglion neurones. *J Physiol* 377:237–249.

41. Tsunoo A, Yoshii M, Narahashi T (1986) Block of calcium channels by enkephalin and somatostatin in neuroblastoma-glioma hybrid NG108-15 cells. *Proc Natl Acad Sci USA* 83(24):9832–9836.

42. Wiley JW, Moises HC, Gross RA, MacDonald RL (1997) Dynorphin A-mediated reduction in multiple calcium currents involves a G(o) alpha-subtype G protein in rat primary afferent neurons. *J Neurophysiol* 77(3):1338–1348.

43. Raingo J, Castiglioni AJ, Lipscombe D (2007) Alternative splicing controls G protein-dependent inhibition of N-type calcium channels in nociceptors. *Nat Neurosci* 10(3): 285–292.

44. Herlitze S, et al. (1996) Modulation of Ca2+ channels by G-protein beta gamma subunits. *Nature* 380(6571):258–262.

45. Qin N, Platano D, Olcese R, Stefani E, Birnbaumer L (1997) Direct interaction of gbetagamma with a C-terminal gbetagamma-binding domain of the Ca2+ channel alpha1 subunit is responsible for channel inhibition by G protein-coupled receptors. *Proc Natl Acad Sci USA* 94(16):8866–8871.

46. Hille B, et al. (1995) Multiple G-protein-coupled pathways inhibit N-type Ca channels of neurons. *Life Sci* 56(11-12):989–992.

47. De Lean A, Stadel JM, Lefkowitz RJ (1980) A ternary complex model explains the agonist-specific binding properties of the adenylate cyclase-coupled beta-adrenergic receptor. *J Biol Chem* 255(15):7108–7117.

48. Li Z, et al. (2014) Activation of MrgC receptor inhibits N-type calcium channels in small-diameter primary sensory neurons in mice. *Pain* 155(8):1613–1621.

49. Heinl C, Drdla-Schutting R, Xanthos DN, Sandkühler J (2011) Distinct mechanisms underlying pronociceptive effects of opioids. *J Neurosci* 31(46):16748–16756.

50. Chen P, Liu Y, Hong Y (2008) Effect of chronic administration of morphine on the expression of bovine adrenal medulla 22-like immunoreactivity in the spinal cord of rats. *Eur J Pharmacol* 589(1-3):110–113.

51. Cai M, Chen T, Quirion R, Hong Y (2007) The involvement of spinal bovine adrenal medulla 22-like peptide, the proenkephalin derivative, in modulation of nociceptive processing. *Eur J Neurosci* 26(5):1128–1138.

52. Jiang J, et al. (2013) Effect of Mas-related gene (Mrg) receptors on hyperalgesia in rats with CFA-induced inflammation via direct and indirect mechanisms. *Br J Pharmacol* 170(5):1027–1040.

53. Ji RR, Kohno T, Moore KA, Woolf CJ (2003) Central sensitization and LTP: Do pain and memory share similar mechanisms? *Trends Neurosci* 26(12):696–705.

54. Woolf CJ, Salter MW (2000) Neuronal plasticity: Increasing the gain in pain. *Science* 288(5472):1765–1769.

55. Bao J, Li JJ, Perl ER (1998) Differences in Ca2+ channels governing generation of miniature and evoked excitatory synaptic currents in spinal laminae I and II. *J Neurosci* 18(21):8740–8750.

56. Perret D, Luo ZD (2009) Targeting voltage-gated calcium channels for neuropathic pain management. *Neurotherapeutics* 6(4):679–692.

57. Klotz U (2006) Ziconotide–a novel neuron-specific calcium channel blocker for the intrathecal treatment of severe chronic pain–a short review. *Int J Clin Pharmacol Ther* 44(10):478–483.

58. Staats PS, et al. (2004) Intrathecal ziconotide in the treatment of refractory pain in patients with cancer or AIDS: A randomized controlled trial. *JAMA* 291(1):63–70.

59. Wermeling DP (2005) Ziconotide, an intrathecally administered N-type calcium channel antagonist for the treatment of chronic pain. *Pharmacotherapy* 25(8): 1084–1094.

60. Hescheler J, Rosenthal W, Trautwein W, Schultz G (1987) The GTP-binding protein, Go, regulates neuronal calcium channels. *Nature* 325(6103):445–447.

61. Kaneko S, et al. (1994) Ca2+ channel inhibition by kappa opioid receptors expressed in Xenopus oocytes. *Neuroreport* 5(18):2506–2508.

62. Bourinet E, Soong TW, Stea A, Snutch TP (1996) Determinants of the G protein-dependent opioid modulation of neuronal calcium channels. *Proc Natl Acad Sci USA* 93(4):1486–1491.

63. Navratilova E, Xie JY, King T, Porreca F (2013) Evaluation of reward from pain relief. *Ann N Y Acad Sci* 1282:1–11.

64. Eisenach JC, Rauck RL, Curry R (2003) Intrathecal, but not intravenous adenosine reduces allodynia in patients with neuropathic pain. *Pain* 105(1-2):65–70.

1   **SUPPLEMENTAL FIGURES, TABLE, AND METHODS**
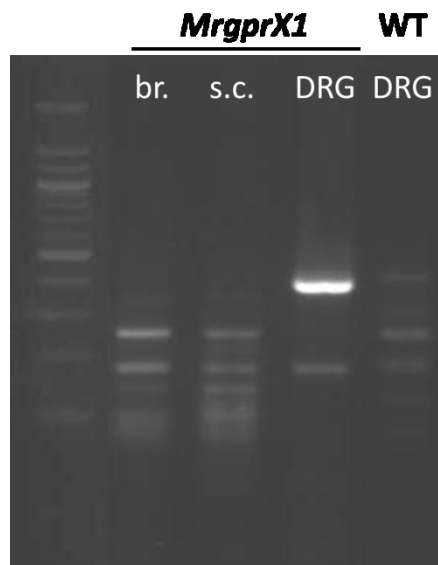
2

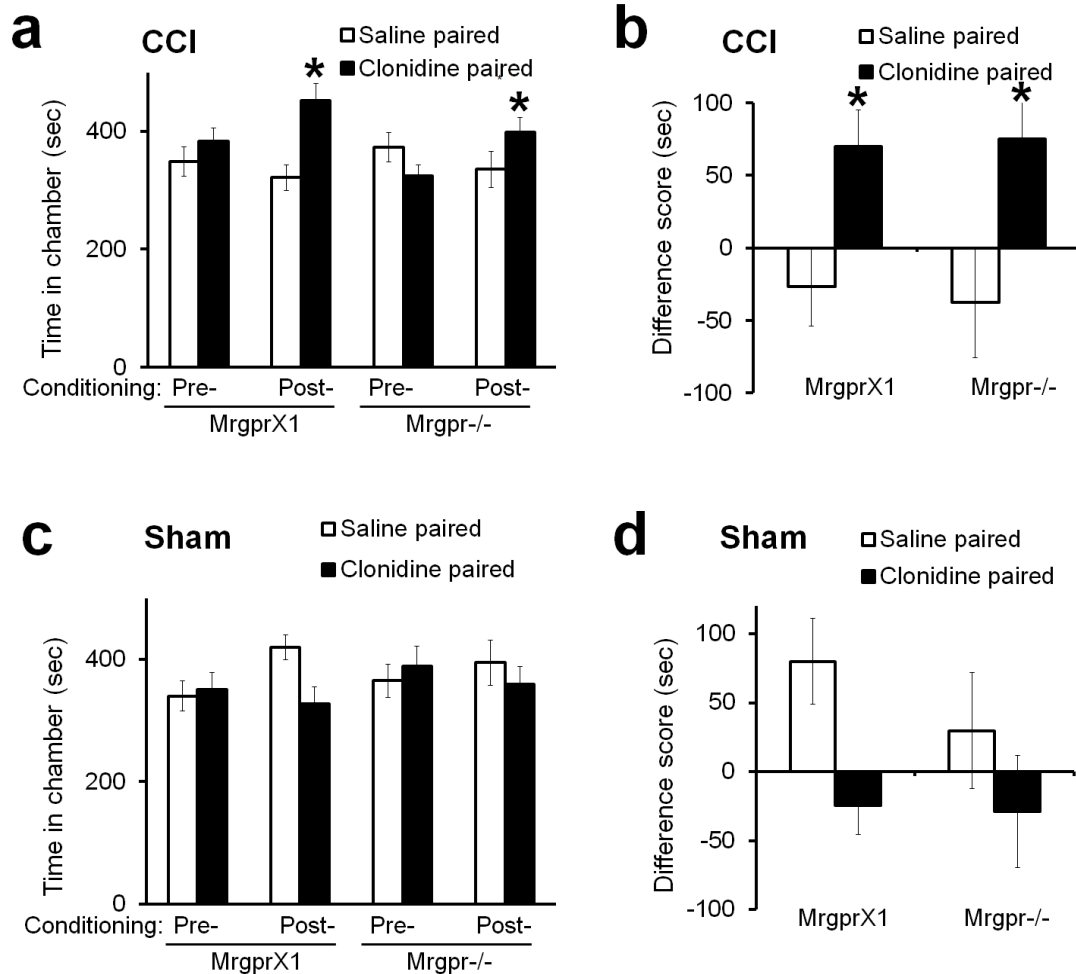3   **SI Appendix, Fig. S1. The expression of *MrgprX1* mRNA in the DRG of humanized**

4   **MrgprX1 mice.**

5   Reverse transcript PCR shows the expression of *MrgprX1* mRNA in dorsal root ganglion

6   (DRG) neurons but not in brain or spinal cord. br.=brain, s.c.=spinal cord, ctrl = DRGs

7   from wildtype (WT) littermate without *MrgprX1* transgene.

8

9

10

1

**SI Appendix, Fig. S2. Positive control of conditioned place preference induced by clonidine after nerve injury**.

(a) Intrathecal administration of clonidine (1 µg, 5 µL saline) induced chamber preference in both *MrgprX1* and *Mrgpr-/-* mice at day 7–13 after chronic constriction injury (CCI) of sciatic nerve (*n*=12/group). *$P<0.05$ vs pre-conditioning. **(b)** The difference score analysis confirmed that both genotypes showed preference for the clonidine-paired chambers. *$P<0.05$ vs. saline. **(c)** The same dose of clonidine did not induce chamber preference in sham-operated mice, regardless of genotype (*n*=12/group). **(d)** The difference score confirmed that neither genotype showed a preference for the clonidine-paired chamber. a,c: Two-way repeated measures ANOVA, with Bonferroni *post hoc* test. b.d: Paired t-test.

2

1
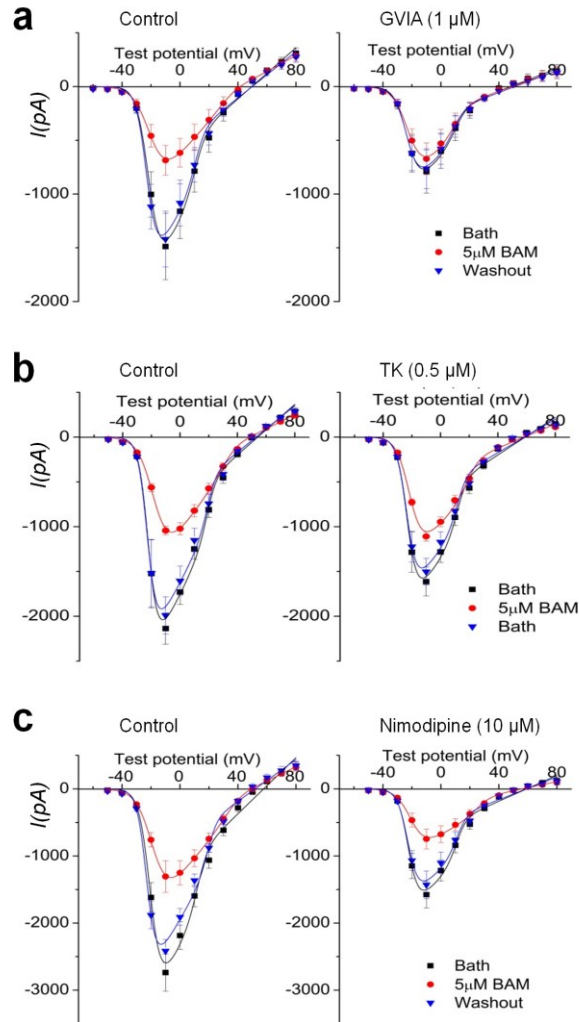
SI Appendix, Fig. S3. Examples of BAM8–22-induced inhibition of different types of high-voltage-activated (HVA) I_{Ca} in DRG neurons from *MrgprX1* mice.

(a) Left: In a control experiment (no blocker, BAM8–22 [BAM] 5 μM) inhibited HVA I_{Ca} by about 50%. Right: N-type HVA calcium channel blocker ω-conotoxin GVIA (1 μM, GVIA) largely abolished BAM8–22-induced HVA I_{Ca} inhibition. **(b)** Left: Without blocker, BAM strongly inhibited HVA I_{ca}. Right: Current-voltage relationship graphs show that ω-agatoxin TK (0.5 μM, TK), a P/Q-type HVA calcium channel blocker, abolished half of BAM8–22-induced HVA I_{ca} inhibition. **(c)** Left: The inhibition of HVA I_{ca} by BAM without blocker. Right: Nimodipine (10 μM), an L-type HVA calcium channel blocker did not reduce BAM8–22-induced HVA I_{ca} inhibition. *n*=5-7 neurons/group.

1
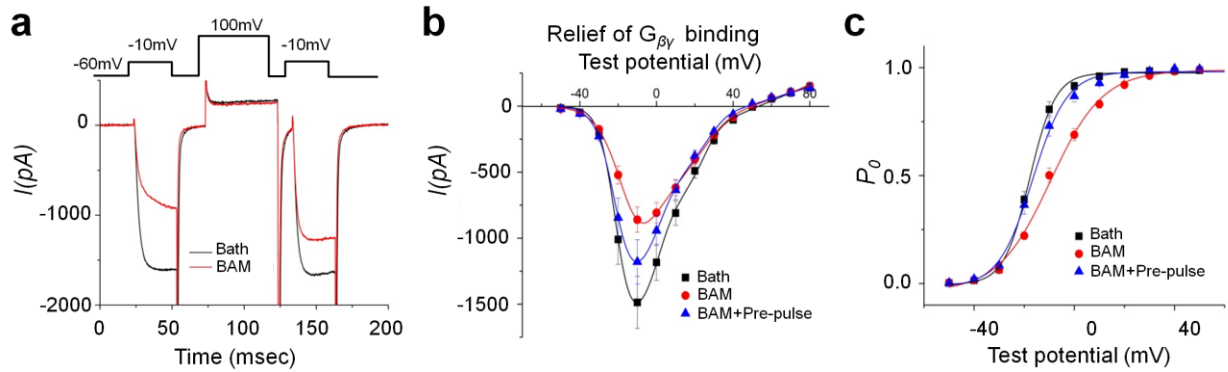
2 **SI Appendix, Fig. S4. Inhibition of HVA I_{Ca} by BAM8–22 partially depends on $G_{\alpha i/o}$-**

3 **sensitive $G_{\beta\gamma}$ binding in DRG neurons from *MrgprX1* mice.**

4 **(a)** A representative trace shows the sandwich stimulation protocol used to relieve $G_{\beta\gamma}$

5 binding to the HVA Ca^{2+} channels with and without bath application of BAM8–22 (BAM,

6 5 μM). **(b)** A graph of the current-voltage relationship shows that the depolarizing pre-

7 pulse reversed 50% of BAM8–22-induced inhibition of HVA I_{ca}. **(c)** Open probability

8 shows that the depolarizing pre-pulse reversed the voltage dependence of the channel.

9 *n*=5-6 neurons /group.

10

11
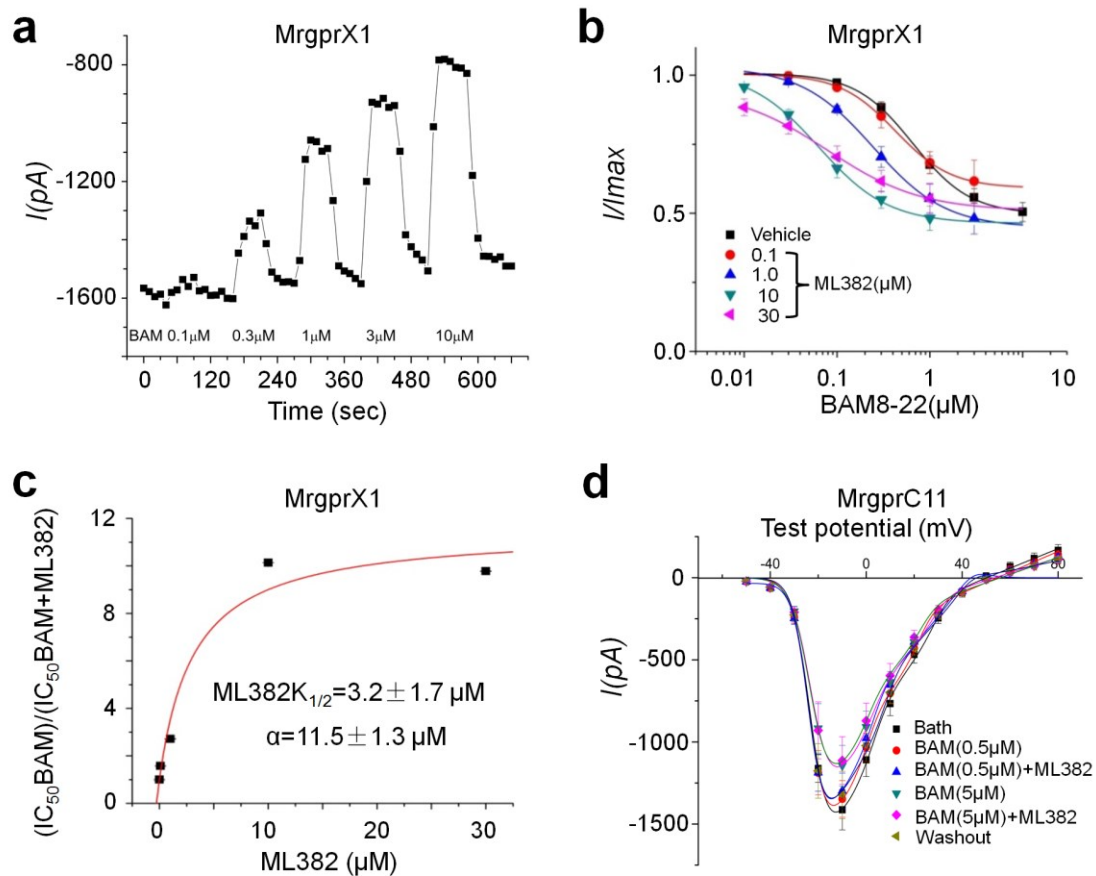
SI Appendix, Fig. S5. Quantification of the potency of ML382 as a positive allosteric modulator for *MrgprX1*.

(a) A representative time course shows the protocol used to measure the dose-response curve of BAM8–22-induced inhibition of HVA I_{ca} in DRG neurons from *MrgprX1* mice. **(b)** IC_{50} of BAM8–22, estimated from the Hill equation in the presence and absence of different concentrations of ML382 (0.1–30 µM) **(c)** The curve used to calculate the EC_{50} and the α value of ML382. **(d)** ML382 did not enhance BAM8–22 inhibition of HVA I_{Ca} through mouse MrgprC11. n=6-8 neurons/group.
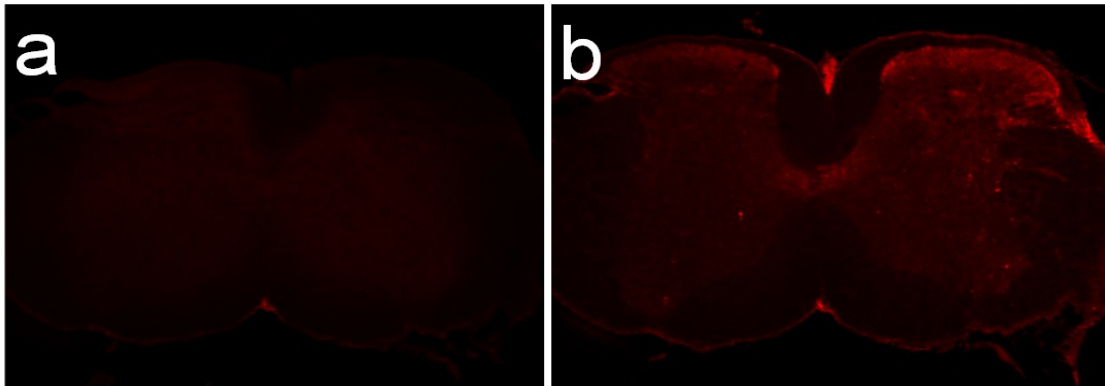
SI Appendix, Fig. S6. Validation of BAM22 antibody.

(a) The anti-BAM22 antiserum was pre-absorbed with 10^{-6} M BAM22, resulting in the absence of BAM22 signal. **(b)** A continuous section of the spinal cord from the same animal was stained with anti-BAM22 antibody that was not pre-absorbed. The BAM22 immunoreactivity is visible on the superficial layers of dorsal horn. The higher signal level on the right side was ipsilateral to the CFA treatment on the hind paw.

1
2
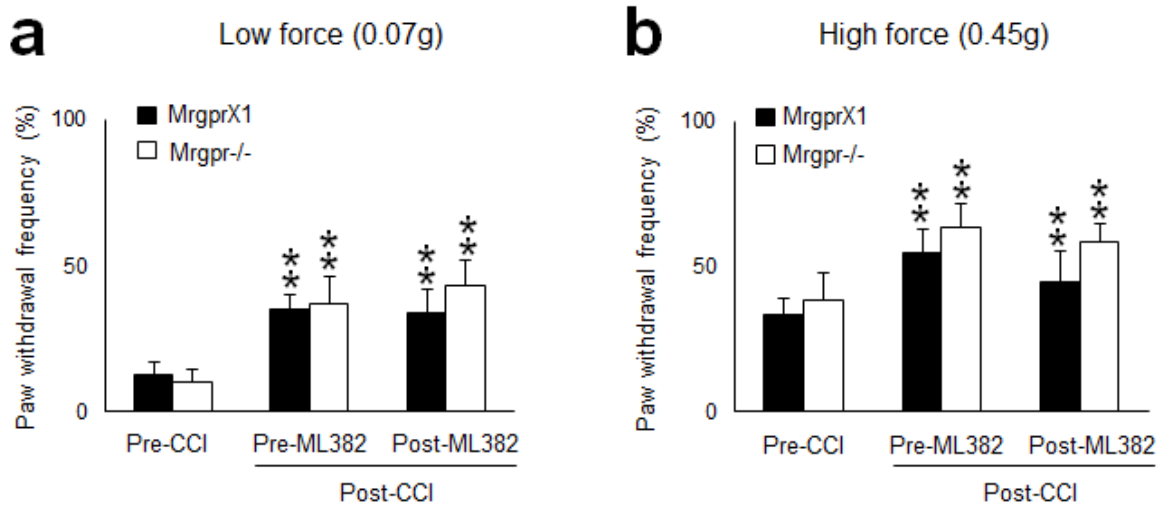
SI Appendix, Fig. S7. Intrathecal injection ML382 did not attenuate mechanical

**hypersensitivity in mice after nerve injury.**

(a) At 2 weeks after chronic constriction injury (CCI) of the sciatic nerve, the paw

withdrawal frequencies (PWF) to a lower force (0.07g) and **(b)** a higher force (0.45g) von

Frey mechanical stimulation applied to the ipsilateral hindpaw were significantly

increased from the respective pre-injury baselines in MrgprX1 (n=8) and Mrgpr-/-mice

(n=6). Intrathecal administration of ML382 (0.25 mM, 5 µL, i.th.) did not significantly

reduce the increased PWF in response to either low-force or high-force stimuli

regardless of genotype. **P < 0.01 vs pre-CCI, two-way mixed model ANOVA with

Bonferroni *post hoc* test.

13

a Formalin test: Post-ML382 (i.p., 8mg/kg)

b

1
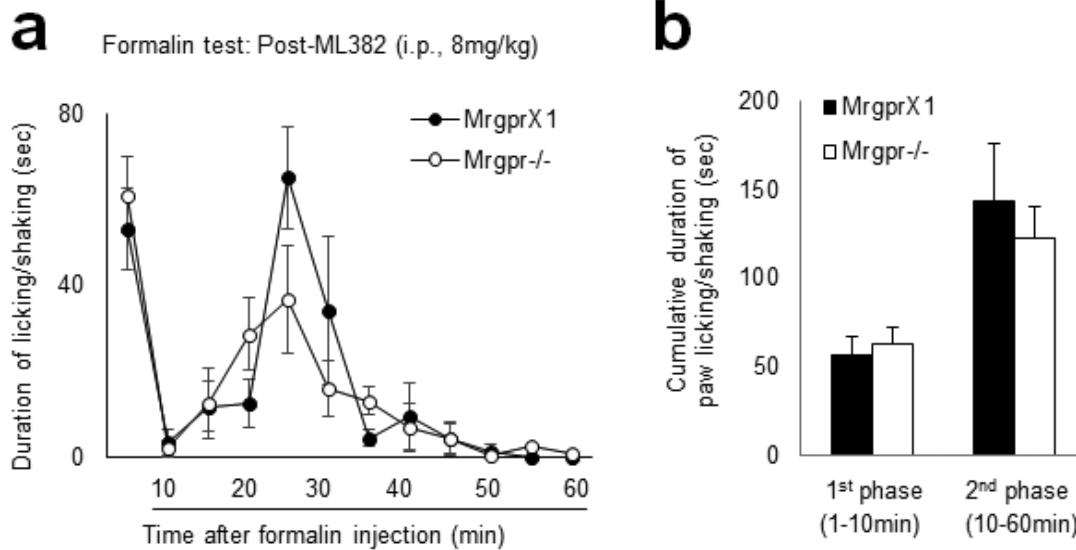
SI Appendix, Fig. S8. Intraperitoneal administration of ML382 did not reduce

formalin-induced pain.

(a) Time course of pain behaviour elicited by intraplantar injection of formalin (2%, 5 µL)

into MrgprX1 and Mrgpr-/- mice that had been pretreated with intraperitoneal injection of

ML382 (8mg/kg, i.p.). **(b)** Cumulative duration of paw licking and shaking after formalin

injection showed that the first and second phases of pain behaviour were not

significantly reduced by ML382 in mice regardless of genotypes. n=8/group, two-way

mixed model ANOVA with Bonferroni *post hoc* test.

1
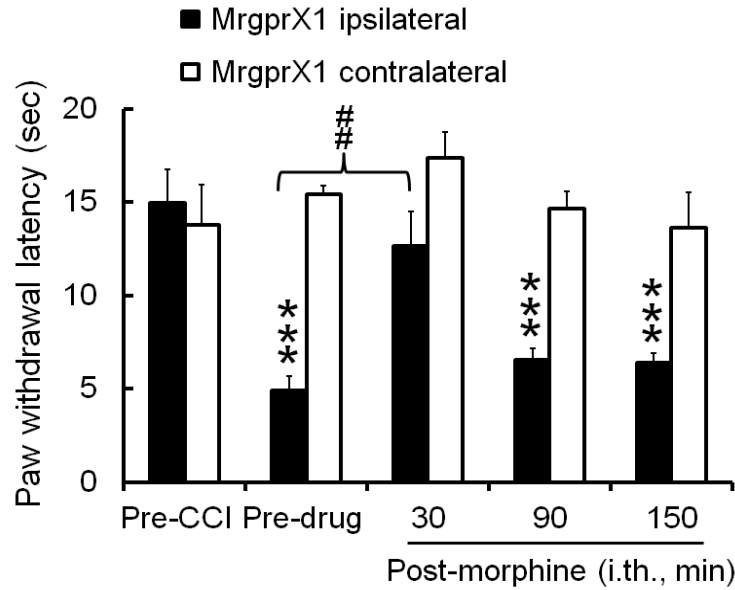
SI Appendix, Fig. S9. Morphine attenuates heat hypersensitivity in MrgprX1 mice

after nerve injury.

At 2 weeks after chronic constriction injury (CCI) of the sciatic nerve, the paw withdrawal

latency (PWL) to radiant heat stimulation was significantly decreased from pre-injury

baseline in the ipsilateral hindpaw of MrgprX1 mice. The heat hypersensitivity in the

ipsilateral hindpaw was attenuated at 30 min after an intrathecal administration of

morphine (5μl, 1mM, i.th.). Contralateral PWL was not altered by CCI or morphine

treatment in MrgprX1 mice. ##P < 0.01 vs pre-drug baseline, ***P < 0.001 vs pre-CCI,

n=8, two-way mixed model ANOVA with Bonferroni *post hoc* test.

Time	Mouse	Rat	Human
0 hr	100%	100%	100%
1 hr	98.47%	102%	103%
4 hr	69.15%	91%	100%

1

2 **Supplemental Table 1. Pharmacokinetic study of ML382.** ML382 was incubated with

3 mouse, rat or human plasma for 0 hr, 1 hr, or 4 hr and then quantified by LC/MC/MC

4 analysis. ML382 was unstable in mouse plasma and stable in rat and human plasma.

1 **SUPPLEMENTAL METHODS**

2 **Reverse transcript PCR**

3 Total RNA was extracted from various tissues using RNeasy Mini Kit (Qiagen) according

4 to the manufacturer's instructions. Reverse transcription was done by Super-Script III

5 First-Strand Synthesis System (Invitrogen). PCR conditions: 95 °C for 3 min, 40 cycles

6 of 30 s at 95 °C, 30 s at 55 °C and 60 s at 72 °C. The primers are located in the human

7 *MrgprX1* exon. The sequence of primers are 5'-TCAACTTGGCCGCAGCAGACTT

8 (forward), 5'-GAGAATCCTGATCAGCAGGACC (reverse).

9 **Analysis of allosterism in functional assay**

10 Dose-response curves were fitted with the Hill equation:

$$E(X) = Emin + \frac{(Emax - Emin) * X^n}{K^n + X^n}$$

11   E(X) is the effect as the function of X (drug concentration). Emin and Emax are

12 the minimum and maximum effects, respectively. K is the equilibrium constant, in this

13 case, the EC_{50}, and n is the Hill coefficient.

14   For mechanistic study of allosteric modulation, a ternary model was used to

15 measure the binding affinity and efficacy of an allosteric modulator. In a ternary complex

16 model with two ligands and one receptor, the interaction within these three molecules

17 can be described with a cyclic model:

$$R \underset{}{\overset{Ka}{\rightleftharpoons}} A + R$$

$$Kb \Updownarrow \qquad\qquad \Updownarrow \alpha Kb$$

$$B + R \underset{\alpha Ka}{\overset{}{\rightleftharpoons}} A + B + R$$
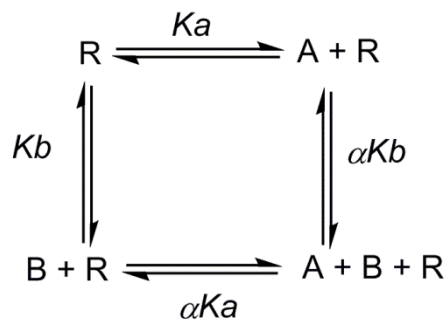
1   In this scheme, R is the receptor, A is the orthosteric ligand, and B is the

2   allosteric modulator. Ka and Kb indicate the association constants of ligands A and B,

3   respectively. When both ligands are interacting with the receptor, they each can

4   reciprocally affect the association constants, and the magnitude of this cooperativity is

5   determined by the factor α. The equation that describes the ternary complex model can

6   be derived from the above scheme and is represented by the following:

$$\frac{K}{K'} = \frac{\alpha[B] + Kb}{[B] + Kb}$$

7   K is the dissociation constant of the orthosteric ligand A, K' is the dissociation

8   constant of the ligand A under the influence of the modulator B, and K_b is the

9   dissociation constant of the allosteric modulator B. The details of the ternary complex

10   model and its derivation can be found in the literature (1-3). If the allosteric modulator

11   does not alter maximum efficacy, the dissociation constant K can represent EC_{50} of the

12   ligand, and the equation can be rewritten in the following form (4):

$$\frac{EC50}{EC50'} = \frac{\alpha[B] + Kb}{[B] + Kb}$$

13   **Plasma Protein Binding**

14   Protein binding of ML382 was determined in human, rat and mouse plasma via

15   equilibrium dialysis employing Single-Use RED Plates with inserts (ThermoFisher

1   Scientific, Rochester, NY). Briefly plasma (220 µL) was added to the 96 well plate

2   containing test article (5 µL) and mixed thoroughly. Subsequently, 200 µL of the plasma-

3   test article mixture was transferred to the cis chamber (red) of the RED plate, with an

4   accompanying 350 µL of phosphate buffer (25 mM, pH 7.4) in the trans chamber. The

5   RED plate was sealed and incubated 4 h at 37 °C with shaking. At completion, 50 µL

6   aliquots from each chamber were diluted 1:1 (50 µL) with either plasma (cis) or buffer

7   (trans) and transferred to a new 96 well plate, at which time ice-cold acetonitrile (2

8   volumes) was added to extract the matrices. The plate was centrifuged (3000 rpm, 10

9   min) and supernatants transferred to a new 96 well plate. The sealed plate was stored at

10 -20 °C until LC/MS/MS analysis.

11 **Quantitative analysis of BAM22 peptide in mouse spinal cord by mass**

12 **spectrometry**

13 BAM22 within the mouse spinal cord was quantified by the LC-SRM approach on our

14 optimized MS platform (5). The spinal cords of CFA- and saline-treated mice were

15 homogenized in lysis buffer (PBS, protease inhibitor cocktail from Roche) at 4 °C with

16 0.5 mm glass beads for 5 min in a Bullet Blender instrument (Next Advance Inc.). The

17 whole lysate was mixed with ice-cold acetonitrile at a final concentration of 80% by

18 vortexing at 20-s intervals for 1 min, and then centrifuged at 21,000 x g for 15 min. The

19 extracted lysate was dried before being dissolved and digested with trypsin (2 µg per

20 spinal cord) in 50 mM HEPES (pH 8.5) at 37oC for 5 h. The digests were acidified with 1%

21 TFA, pre-cleared by centrifugation, and desalted with Sep-Pak C18 SPE column

22 (Waters). The BAM22 tryptic peptides were eluted with 45% acetonitrile plus 1% formic

23 acid. The eluted peptides were dried, reconstituted in 5% formic acid, and analysed on

24 Orbitrap Elite hybrid ion trap MS (Thermo Fisher Scientific), equipped with

25 nanoelectrospray ion source and an Easy-nLC 1000 UHPLC system (Thermo Fisher

13

1 Scientific). Chromatography was performed on a 75 µm x 10 cm picofrit column (New

2 Objective) packed with C18 2.7 µm Halo beads (New Objective). Mobile phases

3 consisted of 0.1% formic acid as solvent A, and 0.1% formic acid/70% acetonitrile as

4 solvent B. The digests were eluted for 20 min at 400 nL/min in a gradient of 30 to 50% B.

5 The LC-SRM was performed with a single Orbitrap MS scan from 350 to 1600 at a

6 resolution of 30,000 with AGC set at 1e5 followed by CID of targeted SRM scans of

7 BAM22 tryptic peptides. For the quantification of BAM22 in mouse spinal cords, the m/z

8 transition of $[M+3H]^{3+}$ precursor ion of $BAM22_{8-19}$ peptide to its product ions was

9 monitored, and the peak areas were calculated by Xcalibur software. Human ubiquitin

10 peptide VGRPEWWMDYQK (100 fmol) was spiked into each run as an internal standard

11 to offset the run-to-run variation. To estimate the absolute amount of BAM22 peptide in

12 the mouse spinal cord, we spiked synthetic BAM22 tryptic digests (250 fmol) into the

13 extracts and analysed them. The peak area of synthetic $BAM22_{8-19}$ peptide was obtained

14 by comparing two runs with or without the spike-in. Relative amounts of BAM22 in CFA-

15 and saline-treated mouse spinal cords were determined by calculating the difference in

16 peak area of multiple SRM transitions of $BAM22_{8-19}$ peptide between the two samples.

17 **Whole-cell voltage-clamp recordings from spinal cord slices.** We used

18 procedures as described previously (48). Briefly, the lumbosacral segment of spinal cord

19 was removed rapidly from CFA-treated MrgprX1 mice or Mrgpr-/- mice and placed in ice-

20 cold, low-sodium Krebs solution (in mM: 95 NaCl, 2.5 KCl, 26 $NaHCO_3$, 1.25 NaH_2PO_4-

21 H_2O, 6 $MgCl_2$, 1.5 $CaCl_2$, 25 glucose, 50 sucrose, 1 kynurenic acid) saturated with

22 95%O_2/5% CO_2. For electrophysiology recording, slices were stabilized with a grid (ALA

23 Scientific, Farmingdale, NY, USA) and submerged in a low-volume recording chamber

24 (SD Instruments, San Diego, CA, USA) that was perfused with room-temperature Krebs

25 solution (in mM: 125 NaCl, 2.5 KCl, 26 $NaHCO_3$, 1.25 NaH_2PO_4-H_2O, 1 $MgCl_2$, 2 $CaCl_2$,

1 and 25 glucose, with 10 µM $GABA_A$ receptor blocker bicuculline and 1 µM glycinergic

2 receptor blocker strychnine) bubbled with a continuous flow of 95% O_2/5% CO_2. Whole-

3 cell patch-clamp recording of lamina II cells was carried out under oblique illumination

4 with an Olympus fixed-stage microscope system (BX51, Melville, NY, USA). Data were

5 acquired with pClamp 10 software (Molecular Devices) and a Multiclamp amplifier. Using

6 a puller (P1000, Sutter, Novato, CA, USA), we fabricated thin-walled glass pipettes

7 (World Precision Instruments) that had a resistance of 3–6 MΩ and were filled with

8 internal solution (in mM: 120 K-gluconate, 20 KCl, 2 $MgCl_2$, 0.5 EGTA, 2 Na_2-ATP, 0.5

9 Na_2-GTP, and 20 HEPES). The cells were voltage clamped at –70 mV. Membrane

10 current signals were sampled at 10 kHz and low-pass filtered at 2 kHz. Larger-bore

11 pipettes filled with Krebs solution were used for dorsal root stimulation. To evoke EPSCs,

12 we delivered paired pulse test stimulation to dorsal root consisting of 2 synaptic volleys

13 (500 µA, 0.1 ms) 400 ms apart at a frequency of 0.05 Hz to activate high-threshold

14 afferent fibres (C-fibres), followed by a 0.1-ms, 5-mV depolarizing pulse (to measure

15 series resistance [R_{series}] and input resistance [R_{input}]). We monitored R_{series} and R_{input} and

16 discarded cells if either of these values changed by more than 20%. The amplitudes of

17 the first (P1) and the second (P2) EPSC were measured, and the paired pulse ratio

18 (PPR) was calculated as PPR = P2/P1.

19 **Immunofluorescence.** For spinal cord staining, adult mice (8–12 weeks old) were

20 anaesthetized with pentobarbital and perfused intracardially with 20 mL of 0.1 M PBS

21 (pH 7.4, 4°C) followed by 25 mL of fixative (4% formaldehyde [vol/vol], 4°C), as

22 previously described (13). Spinal cord was dissected from the perfused mice and post-

23 fixed in fixative at 4°C for 1 h. Then tissues were cryoprotected in 20% sucrose (wt/vol)

24 for 24 h at 4°C and sectioned with a Vibratome cryostat (Polysciences, Warrington, PA).

25 The sections were placed on slides, dried at 37°C for 15 min, and fixed with 4%

1 paraformaldehyde at room temperature for 10 min. We used Tyramide Signal

2 Amplification (TSA; PerkinElmer, Waltham, MA) according to the protocol provided. The

3 sections were incubated with rabbit polyclonal anti-BAM22 antiserum (1:500, ATSBIO,

4 San Diego, CA, USA) (50) in 1×TNB blocking buffer (0.1 M Tris, 0.15 M NaCl, and 0.5%

5 [wt/vol] blocking reagent from PerkinElmer) overnight at 4°C, washed, and then

6 incubated with secondary horseradish peroxidase-conjugated goat anti-rabbit IgG (1:500

7 in 1×TNB, Vector Laboratories, Burlingame, CA, USA) for 1 h. TSA cyanine 3 reagent

8 was added for the amplification step. Images were taken with a Carl Zeiss AXIO

9 Examiner.Z1 confocal microscope (Jena, Germany).

10 **CCI-induced mechanical allodynia**

11 Mechanical sensitivity was assessed with the von Frey test by the frequency method (6).

12 Two calibrated von Frey monofilaments (low force = 0.07 g; high force = 0.45 g) were

13 used. Each von Frey filament was applied perpendicularly to the plantar side of each

14 hind paw for ∼1 s; the stimulation was repeated 10 times to both hind paws. The

15 occurrence of paw withdrawal in each of these 10 trials was expressed as a percent

16 response frequency: PWF = (number of paw withdrawals/10 trials) × 100%.

17 **Itch behavioural study**

18 Mice were acclimatized 1 day before the test. BAM8–22 or ML382 was injected

19 subcutaneously into the nape of the neck (50 µL), intraperitoneally (100 µL), or

20 intrathecally (5 µL). Behavioural responses were video recorded for 30 min. The video

21 recording was subsequently played back in slow motion, and an investigator counted the

22 number of bouts of scratching with the hind paw around the injection site.

23 **Motor function test**

We used the rotarod test to evaluate whether central administration of ML382

affects motor function as previously described (7). All animals were brought to the

behaviour room 10–20 min before the test. The mice habituated in the rotarod apparatus

(Rotamex, Columbus Instruments) at a constant speed of 4 rpm for 10 min 3–5 times on

day 1. Then, on day 2, they received three acceleration training sessions separated by

20 min. Speeds increased from 4 rpm to 40 rpm (with a 4.0-rpm increase every 30 s).

On day 3, they received three trials before drug administration (in the same acceleration

mode as day 2). Then ML382 was applied intrathecally, without isoflurane. The mice

were tested three times beginning 30 min after drug administration. The end point of the

experiment was defined as the time at which the mice fell from the apparatus or rolled

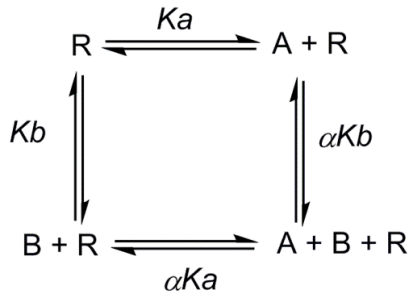over the rod by holding onto it. The latency to the end point was recorded and analysed.

REFERENCES

1. De Lean A, Stadel JM, & Lefkowitz RJ (1980) A ternary complex model explains the agonist-specific binding properties of the adenylate cyclase-coupled beta-adrenergic receptor. *The Journal of biological chemistry* 255(15):7108-7117.
2. Samama P, Cotecchia S, Costa T, & Lefkowitz RJ (1993) A mutation-induced activated state of the beta 2-adrenergic receptor. Extending the ternary complex model. (Translated from eng) *The Journal of biological chemistry* 268(7):4625-4636 (in eng).
3. May LT, Leach K, Sexton PM, & Christopoulos A (2007) Allosteric modulation of G protein-coupled receptors. (Translated from eng) *Annu Rev Pharmacol Toxicol* 47:1-51 (in eng).
4. Ehlert FJ (1988) Estimation of the Affinities of Allosteric Ligands Using Radioligand Binding and Pharmacological Null Methods. (Translated from English) *Mol Pharmacol* 33(2):187-194 (in English).
5. Pagala VR*, et al.* (2015) Quantitative protein analysis by mass spectrometry. *Methods in molecular biology* 1278:281-305.
6. Guan Y*, et al.* (2010) Mas-related G-protein-coupled receptors inhibit pathological pain in mice. (Translated from eng) *Proceedings of the National Academy of Sciences of the United States of America* 107(36):15933-15938 (in eng).
7. Han L*, et al.* (2013) A subpopulation of nociceptors specifically linked to itch. (Translated from eng) *Nature neuroscience* 16(2):174-182 (in eng).

1 **Appendix**

$$R \xrightleftharpoons[]{Ka} A + R$$

with vertical arrows Kb and αKb, and bottom

$$B + R \xrightleftharpoons[\alpha Ka]{} A + B + R$$

2

3 $\quad K_a = \dfrac{[AR]}{[A][R]}$

4 $\quad K_b = \dfrac{[BR]}{[B][R]}$

5 $\quad \alpha K_a = \dfrac{[ARB]}{[A][BR]}$

6 $\quad \alpha K_b = \dfrac{[ARB]}{[B][AR]}$

7 $\quad [Rt] = [R]+[AR]+[BR]+[ABR]$

8 $\quad$ Fraction of binding (ρ) $= \dfrac{[AR]+[ABR]}{[R]+[AR]+[BR]+[ABR]}$

9 $\quad$ Since $[AR] = Ka[A][R]$, $[BR] = Kb[B][R]$, $[ABR] = \alpha KaKb[A][B][R]$

10 $\quad \rho = \dfrac{Ka[A][R]+\alpha KaKb[A][B][R]}{[R]+Ka[A][R]+Kb[B][R]+\alpha KaKb[A][B][R]} = \dfrac{[A](1+\alpha Kb[B])}{\frac{1}{Ka}+[A]+\frac{Kb}{Ka}[B]+\alpha Kb[A][B]} = \dfrac{[A](1+\alpha Kb[B])}{[A](1+\alpha Kb[B])+\frac{1+Kb[B]}{Ka}}$

11 $\quad = \dfrac{[A]}{[A]+\frac{1+Kb[B]}{Ka(1+\alpha Kb[B])}}$

12 $\quad$ Dissociation constants $K_A = 1/K_a$ and $K_B = 1/K_b$

13 $\quad \rho = \dfrac{[A]}{[A]+\frac{KA(1+\frac{[B]}{KB})}{1+\frac{\alpha[B]}{KB}}} = \dfrac{[A]}{[A]+KA'}$

1     $K_A{'}$ is the apparent dissociation constant of [A] in the presence of [B].

2     $K_A{'} = \dfrac{KA(1+\frac{[B]}{KB})}{1+\alpha\frac{[B]}{KB}} = \dfrac{KA(KB+[B])}{KB+\alpha[B]}$

3     $\dfrac{KA}{KA'} = \dfrac{\alpha[B]+KB}{[B]+KB}$

4